CFD modeling of traffic tidal flow

CFD modeling of traffic tidal flow: assessment of pollutant dispersion

Zhengtong Li

c. Department of Aeronautical and Aviation Engineering, The Hong Kong Polytechnic University, Hong Kong, China

Tingzhen Ming

a. School of Architectural Engineering, Huanggang Normal University, No. 146 Xingang Second Road, Huanggang 438000 China.

b. School of Civil Engineering and Architecture, Wuhan University of Technology, Wuhan 430070, China.

Tianhao Shi

b. School of Civil Engineering and Architecture, Wuhan University of Technology, Wuhan 430070, China

Hao Zhang

d. School of Professional Education and Executive Development, The Hong Kong Polytechnic University, Hong Kong, China

Chih-Yung Wen

c. Department of Aeronautical and Aviation Engineering, The Hong Kong Polytechnic University, Hong Kong, China

Yongjia Wu

b. School of Civil Engineering and Architecture, Wuhan University of Technology, Wuhan 430070, China

Caixia Wang

b. School of Civil Engineering and Architecture, Wuhan University of Technology, Wuhan 430070, China

Kui Yin

e. China Construction Third Bureau First Engneering CO .,LTD, Wuhan 430040, China

Renaud de Richter

f. Tour-Solaire.Fr, 8 Impasse des Papillons, F34090 Montpellier, France

Wei Li

g. Institute for Materials and Processes, School of Engineering, The University of Edinburgh, Edinburgh EH9 3FB, Scotland, UK

Corresponding author:

Tingzhen Ming, Professor, School of Architectural Engineering, Huanggang Normal University, No. 146 Xingang Second Road, Huanggang 438000 China, Email: tzming@whut.edu.cn

Abstract: Pollutant distribution remains poorly understood when traffic tidal flows (TTFs) happen. By conducting computational fluid dynamic (CFD) simulations, the research efforts first focus on how different-side traffic-produced flow and turbulence (TPFT) affect in-canyon airflow and corresponding pollutant dispersion. Second, the composite effects of non-uniform traffic emission and TPFT are investigated. Finally, the influences of TTFs while varying different street canyon geometry and approaching wind condition is explored.

The results demonstrate that the turbulent diffusion terms enhanced by the traffic movement contribute to the pollutant dispersion around traffic lanes. Besides, both-side TPFTs push leeward pollutants towards traffic flow "downstream" due to the unidirectional advection terms along the traffic direction. Simultaneously considering the non-uniform traffic emission and TPFT, either leeward- or windward-congested TTFs has a higher concentration at the pedestrian level close to the congested traffic lane. Besides, the TTF with windward congestion has a higher volume-average concentration of the whole street canyon. With varying building separation, street canyon aspect ratio, and incoming wind direction, the TTFs still result in a larger pollutant accumulation above the pedestrian level, which is nearby the congested traffic flow.

Keywords: Street canyon; Traffic-produced flow and turbulence; Traffic tidal flow; Computational fluid dynamics (CFD).

List of acronyms

ABL	Atmospheric boundary layer
GCI	Grid-convergence index
RANS	Reynolds-averaged Navier–Stokes
SF_6	Sulfur hexafluoride
SKE	Standard k-ε
TKE	Turbulent kinetic energy
TPFT	Traffic-produced flow and turbulence
TTF	Traffic tidal flow
UDS	User Defined Scalar
WT	Wind tunnel

1. Introduction

The ongoing global urbanization and highly intensive traffic emissions have arisen numerous environmental problems (Grimmond, 2007; Peng et al., 2015), hence are considerably affecting public health (e.g., respiratory and lung diseases) (Rückerl et al., 2011) and even causing significant economic loss (Xia et al., 2016). Annually, nearly three million people die prematurely due to increasingly deteriorated air quality around the world (Who, 2014). This should be attributed to the dramatically increased demands of civil motor vehicles because of great population growth (Zhou and Lin, 2019), emitting an enormously high intensity of air pollutants (Shi et al., 2018). Thus, there is a more imminent need to solve this problem, which calls for the creation of a cleaner (less air pollution) outdoor urban environment (Ming et al., 2017; Wang et al., 2021).

Unexpected traffic delays, accidents, and breakdowns disturb and interrupt the regular traffic flow, making the urban air pollution issue more serious (Anjum et al., 2019). Thus, road characteristics and traffic patterns are directly related to the local air quality (Wai et al., 2012). The traffic tidal flow (TTF) phenomenon has increasingly become a concerning problem. This phenomenon is widely observed or reported in

many megacities in China, e.g., Beijing (Chen et al., 2019), Changsha (Li et al., 2015), and Wuhan (our previous study) (Ming et al., 2018). It has gradually become one of the most important components of urban traffic congestion during peak commute periods (Yao et al., 2018). TTF, characterized by a very heavy traffic flow on one side and an unobstructed traffic flow on the other during rush hours, occurs when the commercial and residential areas are separated by urban development (Issakhov and Omarova, 2021; Ming et al., 2018). So, two-side traffic flows are heavily imbalanced, causing the traffic tidal flows (TTFs) phenomenon as a result (Li et al., 2020; Ming et al., 2018), as illustrated in Figure 1(a). Massive research has been conducted to mitigate the TTF phenomenon through traffic flow control (Ampountolas et al., 2020; Hu et al., 2021). However, the pollutant distribution remains poorly understood when the TTFs happen. In the existing studies, only the non-uniform emission intensity (Figure 1 (b)) is taken into consideration (Issakhov and Omarova, 2021; Li et al., 2020; Ming et al., 2018). However, the non-uniform vehicle speed and traffic volume due to TTFs also result in non-uniform traffic-produced flow and turbulence (TPFT), as seen in Figure 1 (b).

Although only a few pieces of literature deal with the influence of TPFT within urban areas, its importance in determining pollutant distribution is confirmed (Shi et al., 2020). Rastetter (Rastetter, 1997) and Kastner-Klein et al. (Kastner-Klein et al., 2000) stated that the influence of inflow wind conditions and moving vehicles on the pollutant dispersion was of the same order. Without considering the traffic movement, the pollutant concentration in a street canyon will be underestimated (Cai et al., 2020a; Mazzeo and Venegas, 2005; Sahlodin et al., 2007; Zhao et al., 2021).

Several major aspects of the TPFT have been studied in the literature, 1) vehicle speed (Shi et al., 2020; Wang et al., 2019), 2) traffic composition (one-way or two-way)(Pospisil and Jicha, 2010; Wang and Zhang, 2009; Zheng and Yang, 2022), 3) vehicle shape (truck, SUV and car)(Cai et al., 2020a), 4) traffic density (Rakowska et al., 2014) or traffic-flow patterns (free-flow, interrupted-flow, and congested-flow)(Thaker and Gokhale, 2016). Most of these previous studies focus on identical

traffic conditions in both-side traffic directions. Thus, these studies hold the same vehicle speed and volume for a two-way traffic flow. However, much less is known about non-uniform TPFT on the distribution of pollutants in urban areas.

To fill the above research gaps, the present research aims (i) to solely investigate the potential contribution of the leeward and windward TPFT to find out how different-side traffic motion affects pollutant dispersion; (ii) to jointly consider the non-uniform pollutant emission and non-uniform TPFT induced by TTFs to analyze the pollutant distribution; (iii) to explore the influence of TTFs when the street canyon geometry and incoming wind condition vary.

The remaining contents of this paper are structured as follows: In section 2, a previous wind-tunnel experiment for the validation is briefly outlined. Section 3 establishes the methodological framework, presenting the simulation details of the computational fluid dynamic (CFD) setup. The present computational model is validated in section 4. Section 5 firstly discusses the influence of traffic movement above different sides by analyzing their impact on the mean flow, turbulence, and pollutant distribution. A budget analysis is also conducted to estimate the contribution of advection and turbulent diffusion for pollutant transport. Furthermore, the influence of TTFs is explored when varying the building separation, building height, and incoming wind direction. Finally, the conclusions and limitations are given in section 6.

(a)

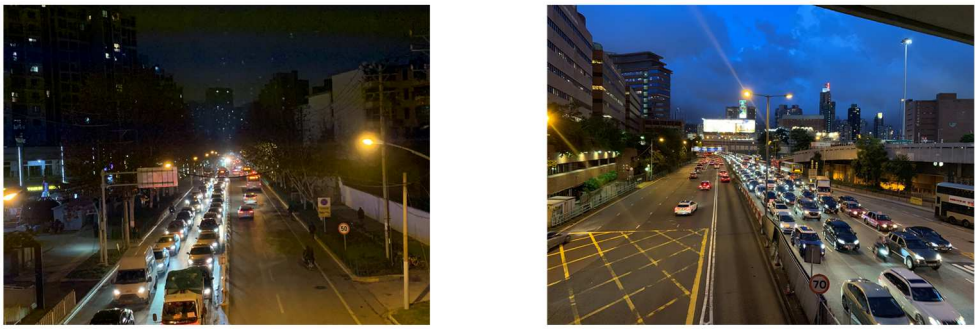

Wuhan, China HongKong, China

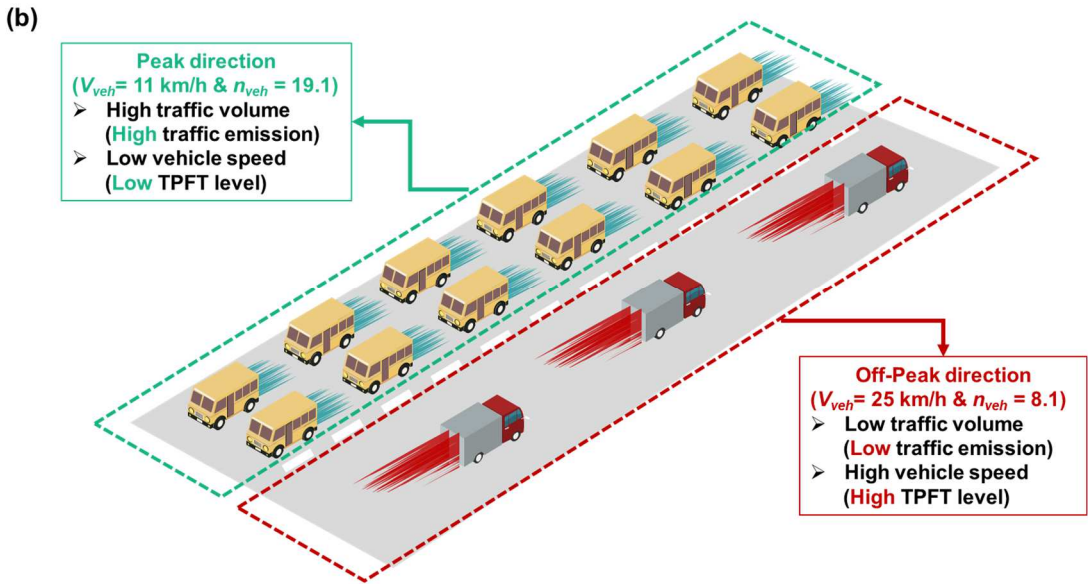

Figure 1 (a) Photos of TTFs in the realistic urban areas by authors and (b) schematic illustrating the non-uniform traffic emission and non-uniform TPFT caused by TTFs.

2. Description of wind tunnel experiments

The current computational model to reproduce the flow and concentration fields affected by moving vehicles is justified by a wind tunnel experiment (WT). This experiment is conducted earlier at the Laboratory of Building and Environmental Aerodynamics, University of Karlsruhe (Gromke, 2013; Gromke and Ruck, 2007). As seen in Figure 2, a scaled model (1:150) of a three-dimensional isolated street canyon with the dimension of height (H) × width (W)× length (L) = 0.12 m × 0.12 m × 1.2 m is tested. The isolated street canyon is simulated in a neutral atmospheric boundary layer (ABL) with the power-law exponent of 0.30 for wind speed and -0.36 for turbulence intensity. The wind speed and turbulence intensity profile of the approaching flow can be approximated by using the following power-law form,

$$U(z) = U_{ref} \times (z / 0.1m)^{0.3} \quad (1)$$

$$I(z) = I_{ref} (z / 0.1m)^{-0.36} \quad (2)$$

where the reference wind speed U_{ref} is 4.39 m/s and the reference turbulence intensity I_{ref} is 17.3%.

Inside the street canyon, two circulating belts are installed on the floor to model the two-way traffic produced flow and turbulence (Figure 2). A group of small plates at 0.1m intervals are mounted on two circulating belts, which represents a vehicle density of 6.67 cars per 100 m in the full scale. The moving speed of circulating belts is set as 11.1 m/s on both lanes. The sulfur hexafluoride (SF_6) is chosen as the tracer gas to model the release of traffic emission. The SF_6 is emitted from four wirelike pollutant sources with an area of 1.42 m (l)× 0.003 m, with an emission rate (Q) of 10 g/s. The measurement of pollutant concentration is located 5mm away from the building surfaces (Buccolieri et al., 2009; Zheng and Yang, 2021). The concentration of SF_6, C, is presented as the dimensionless concentration C^+, as follow,

$$C^+ = \frac{CU_{ref}H}{Q/l} \tag{3}$$

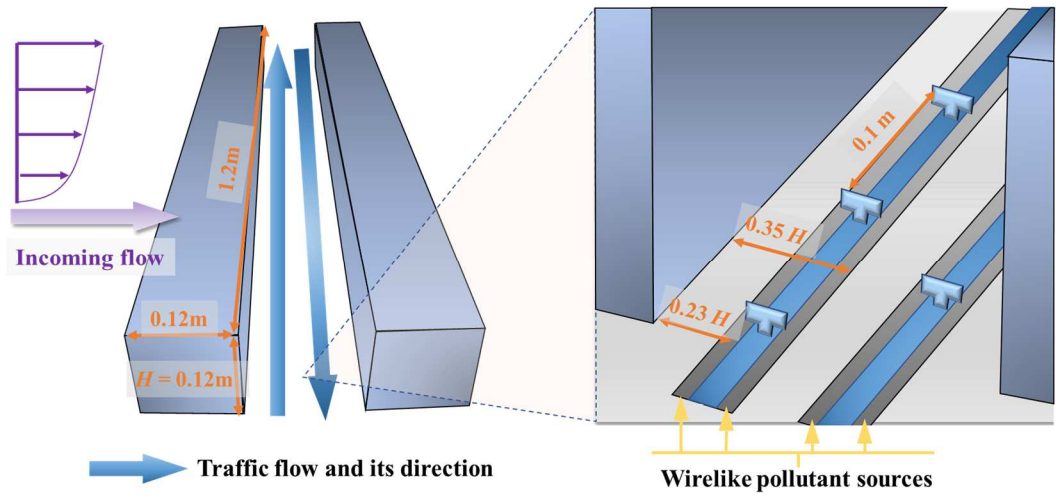

Figure 2. Schematics of the WT with an urban street canyon (scale 1:150) and two circulating belts for moving vehicles simulation (Gromke, 2013; Gromke and Ruck, 2007)

3. Methodology

3.1 Description of computational geometry, grid and case studies

The street canyon configurations used in the CFD simulations are constructed based on the scaled model (1:150) of an isolated street canyon adopted in the WT

mentioned above. The size and discretization of the computational domain are based on the geometry setting of the WT. The distances between the building and the inlet boundary, top boundary, lateral boundaries, and outflow boundary are 1.2 m (10*H*), 0.96 m (8*H*), 0.36 m (3*H*), and 1.8 m (15*H*), respectively, which is in line with Ref(Franke et al., 2011; Tominaga et al., 2008; Zheng et al., 2021). The origin of coordinates is at the center of the floor edge of the inlet boundary.

In the position of moving vehicles, two rectangular solid volumes are assumed to represent the directly affected region, in which the additional source terms of Eq. (4) & (7) are switched on. Considering the heavily imbalanced traffic caused by the TTF, we differentiate the leeward source (colored by blue) and the windward source (colored by green).

The computational domain is discretized into about six million hexahedral cells (Figure 3(b)). There are relatively large gradients of the velocity near the ground and building surfaces and more intricate flow morphologies caused by moving traffic. Cubic cells with $\Delta x = \Delta y = \Delta z = H/40$ are set for the region within the street canyon (Figure 3(b)). Besides, a grid-sensitivity analysis is performed based on two additional grids: a coarser grid and a finer grid. For the coarse, basic, and fine grids, the minimum sizes are set to be $H/50$, $H/40$, and $H/20$, respectively. The total cell numbers for the coarse, basic, and fine grids are 1.4 million, 6.6 million, and 12.2 million, respectively. Then, the results of grid-sensitivity analysis discussed later (Appendix A2) indicate that the basic grid provides nearly grid-independent results, which can be further used for the remainder of this study.

Besides the uniform two-way traffic flow studied by the WT, this study focuses on the non-uniform traffic flow. To have an in-depth understanding of TTFs in the following case studies, at first, the influence of leeward and windward traffic movement is solely explored. In this section, the traffic condition of each traffic flow is the same as the setting of the WT, i.e., V_{veh} = 11.1 m/s & n_{veh} =10. Herein, V_{veh} is the average vehicle speed and n_{veh} is the number of vehicles per unit length per lane, which will be

discussed later in Section 3.4. The intensity of the pollutant source is also identical to the WT (Q = 10 g/s). Then, the TTFs are modeled based on our previous observation and statistics (Ming et al., 2018). In this previous study, two typical TTFs differentiated by the varying locations of congestion are recorded, i.e., the leeward-congestion TTF and the windward-congestion TTF. There is a lower vehicle speed (V_{veh} = 11 km/hour) and a higher traffic density (n_{veh} = 19.1) for the congested traffic flow, while a higher vehicle speed (V_{veh} = 25 km/hour) and a lower traffic density (n_{veh} = 8.1) for the non-congested traffic flow, as seen in Figure 1(b). The ratio of emission rate for the congestion side and non-congestion side is about 2 (as seen in Table A1). Since the present study considers the dimensionless concentration, the intensity of the pollutant source for the congestion side is ideally set as 20 g/s while 10 g/s for the non-congestion side. The street canyon geometry (H/W =1) and inlet boundary condition are in line with the WT for this section. Furthermore, the influences of TTFs under different conditions are investigated, including different building separations, the different aspect ratios of the street canyon, and different incoming wind directions.

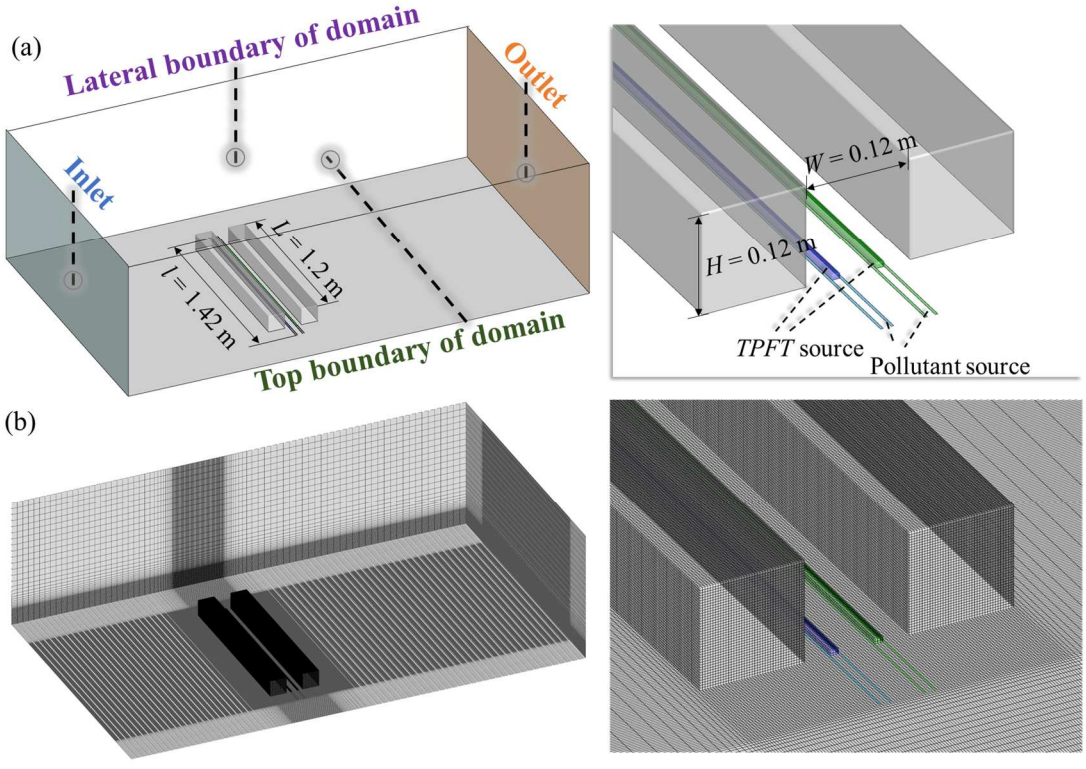

Figure 3 (a) The geometric model, computational domain, and boundary conditions and (b) Grid distributions

3.2 Governing equation and turbulence model

The analyses are based on the steady-state 3D Reynolds-averaged Navier–Stokes (RANS) conservation equations of mass and momentum for the incompressible turbulent flow. The governing equations are as follows:

Continuity equation:

$$\frac{\partial u_i}{\partial x_i} = 0 \tag{4}$$

Momentum equation:

$$\frac{\partial(\rho u_i u_j)}{\partial x_j} = -\frac{\partial p}{\partial x_i} + \frac{\partial \tau_{ij}}{\partial x_j} + \rho g_i + S_{u_i} \tag{5}$$

where the stress tensor τ_{ij} is defined as:

$$\tau_{ij} = \rho\left[\nu_t\left(\frac{\partial u_i}{\partial x_j} + \frac{\partial u_j}{\partial x_i}\right)\right] - \frac{2}{3}\rho k \delta_{ij} \tag{6}$$

where the u_i denotes the i-axis component of the air velocity; p and ρ represent the pressure and density; ν_t is the turbulent kinematic viscosity; δ_{ij} is the Kronecker delta; k is the turbulence kinetic energy. S_{ui} is the additional source term of the momentum equation due to the traffic flow, which will be elaborated in Section 3.4.

The species transport equation is solved to model the pollutant dispersion in an urban environment as follows:

$$\frac{\partial u_i Y}{\partial x_i} - \frac{\partial}{\partial x_i}\left[\left(D + D_t\right)\frac{\partial Y}{\partial x_i}\right] = S_p \tag{7}$$

where D and D_t (= ν_t/Sc_t) denote the molecular and turbulent diffusion coefficients of the pollutant, respectively. Sc_t is the turbulent Schmidt number, which is set to 0.3 to account for the underestimation of the turbulent mass diffusion from the RANS models (Hang et al., 2012; Tominaga and Stathopoulos, 2007; Zheng and Yang, 2021). Y is the

mass fraction of the pollutants. This dispersion of pollutants is simulated with the User Defined Scalar (UDS) option in ANSYS Fluent.

The standard *k*-*ε* (SKE) turbulence model has been demonstrated to be capable of simulating a wide range of turbulent flow phenomena for effectively characterizing the airflow and pollutant transport in street canyons (Tan et al., 2015). According to the simulation study conducted by Zheng and Yang (Zheng and Yang, 2021), it is found that the SKE turbulence model can yield the best agreement with the same WT data using a similar traffic movement model, compared to other RANS models (Reynolds stress model (RSM), shear stress transport (SST) k-ω model, renormalization group (RNG) k-ε model and realizable k-ε model (RKE)). Thus, the standard *k*-*ε* model is used to solve this steady-state flow field affected by the traffic movement. The conservation equations of the standard *k*-*ε* turbulence model for the turbulence kinetic energy (*k*) and dissipation rate (*ε*) are as follows:

$$\frac{\partial u_j k}{\partial x_j} = \frac{\partial}{\partial x_j}\left[\left(\nu + \frac{\nu_t}{\sigma_k}\right)\frac{\partial k}{\partial x_j}\right] + P - \varepsilon + S_k \tag{8}$$

$$\frac{\partial u_j \varepsilon}{\partial x_j} = \frac{\partial}{\partial x_j}\left[\left(\nu + \frac{\nu_t}{\sigma_\varepsilon}\right)\frac{\partial \varepsilon}{\partial x_j}\right] + C_{\varepsilon 1}\frac{P\varepsilon}{k} - C_{\varepsilon 2}\frac{\varepsilon^2}{k} \tag{9}$$

The production term is defined as:

$$P = \nu_t\left(\frac{\partial u_j}{\partial x_i} + \frac{\partial u_i}{\partial x_j}\right)\frac{\partial u_j}{\partial x_i} \tag{10}$$

Here, the values of the constants C_μ, σ_k, σ_ε, $C_{\varepsilon 1}$, and $C_{\varepsilon 2}$ are 0.09, 1.44, 1.92, 1.0, and 1.3, respectively. Besides, S_k denotes the additional term of turbulent kinetic energy induced by traffic flow, which will be explained in Section 3.4.

3.3 Boundary conditions

At the domain inlet, the measured inlet velocity and turbulence intensity profile from the WT is used to model a neutral ABL. The turbulent kinetic energy *k* and turbulence dissipation rate *ε* profiles are applied as follows,

$$k(z) = \left(U(z) \times I_{in}\right)^2 \tag{11}$$

$$\varepsilon(z) = \frac{C_\mu^{3/4} k(z)^{3/2}}{\kappa z}, \tag{12}$$

where κ is the von Karman's constant (≈ 0.4) and C_μ is the model constant (= 0.085).

The Reynolds number ($\mathrm{Re} = U_{ref} H / \nu$) for the regular street canyon is about 3.6×10^4, which is larger than 11,000 to satisfy the requirement of Reynolds number independence (Snyder, 1972). For the deep street canyon, its Reynolds number is about 7.2×10^4 also can meet the requirement of Reynolds number independence for the scale deep street canyon with height aspect ratio =2 (57,000) (Chew et al., 2018).

Besides, as seen in Figure 3(a), the bottom, top and lateral boundaries of the domain are set as no-slip walls, namely reproducing the floor, ceiling, sidewalls of the WT test section. On the outlet of the domain, a zero diffusive flux is imposed for all flow variables in the direction normal to the outflow plane since the domain downstream is long enough to ensure a fully developed outlet flow.

3.4 Modeling traffic-produced flow and turbulence

The representation of traffic movement in the CFD model is crucial to capture their effects on wind flow insides the street canyon (Cai et al., 2020b; Kondo and Tomizuka, 2009). Besides the dynamic mesh updating technology to simulate the characteristics of moving vehicles adopted by our research team (Cai et al., 2020b; Li et al., 2017; Shi et al., 2020; Wang et al., 2019), the aerodynamic effects of the inclusion of traffic movement can be also modeled by an explicit method in the literature (Mochida and Lun, 2006). This method to model traffic movement is defined as a "vehicle canopy model" (Mochida and Lun, 2008). Without directly modeling each individual moving vehicle, the total effects of all the moving vehicles above traffic lanes are treated as a whole (Mochida and Lun, 2008). Their aerodynamic effects are modeled using the methodology of canopy model; thus the additional terms are added to basic equations

for the momentum (S_i) and the turbulent kinetic energy (S_k) (Kondo and Tomizuka, 2009; Mochida and Lun, 2008; Thaker and Gokhale, 2016; Zheng and Yang, 2021),

$$S_i = \frac{1}{2}\rho C_d \frac{A_{veh}}{A_{cel}} n_{veh}(V_{veh,i} - u_i)\left|V_{veh,i} - u_i\right| \quad (13)$$

$$S_k = S_i(V_{veh,i} - u_i) \quad (14)$$

where following the setup of the WT, C_d is the drag coefficient of the vehicle (= 1.2), A_{veh} is the frontal vehicle area (= 50 mm^2); A_{cel} is the cross-section of control volumes pass by vehicles (= 54 mm^2). n_{veh} is the number of vehicles per unit length per lane and $V_{veh,i}$ is the vehicle speed in the i direction.

3.5 Solver settings

The commercial software ANSYS/Fluent® CFD software (Release 15.0) (Fluent, 2013) is used to simulate the airflow of ambient wind over this isolated street canyon. This study utilizes the pressure-linked equations-consistent (SIMPLEC) numerical method for the pressure-velocity coupling. The second-order upwind scheme (Barth and Jespersen, 1989) is used to discretize both the convective terms and the diffusion terms. A double-precision solver is also selected for the CFD calculations. The convergence criterion of the normalized residual errors is set to 10^{-6} for the governing equations.

4. Validation study

A cross-comparison of the dimensionless wind velocity and pollutant concentration on the building surface between the numerical and experimental results (personal communication with Dr. Christof Bernhard Gromke) is presented in Figure 4 (a)–(c) (the comparisons in more positions are supplemented in Figure A7 (a)–(c)). On the corner plane, the results of predicted streamwise flow velocities agree well with the experimental data (Figure 4(a) and Figure A7(a)). However, the present simulation underestimates the negative spanwise airflow, which means the lateral entrainment through the lateral boundary (Figure 4(a) and Figure A7(a)). This is due to the weakness of the RANS model to predict the wake region of the leeward building (Hayati et al.,

2019). Therefore, there is a thinner sidewall boundary layer and weaker lateral entrainment when the RANS model is used (Hayati et al., 2019). On the central plane, the present simulation reasonably predicts the streamwise flow velocities (Figure 4(b) and Figure A7(b)). Nonetheless, there still is an underprediction of vertical wind velocities on this central plane (Figure 4(b) and Figure A7(b)). This is because the RANS model underpredicts the strength of the in-canyon circulation (the main vortex) (Salim et al., 2011). Figure 4(c) and Figure A7(c) graphically presents the concentration profiles at several different vertical locations along both walls. The present simulation provided consistent predicted results against the WT, doing well at all locations along the leeward building surface and only slightly overpredicting on the windward building surface. Besides, on the leeward surface, the traffic-induced skewness of pollutant concentration, which shifts towards the traffic direction of the leeward traffic flow, is well simulated by the present CFD model. Overall, it could be concluded that the present CFD simulation method is able to perform well in capturing the spatial distribution of the pollutant affected by the moving traffic.

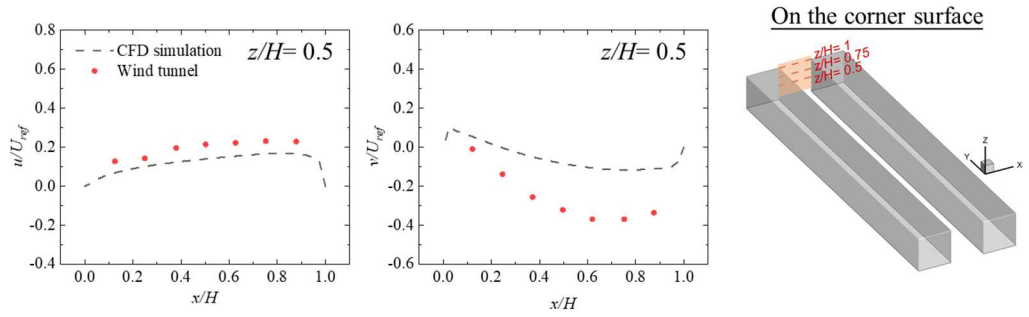

(a)

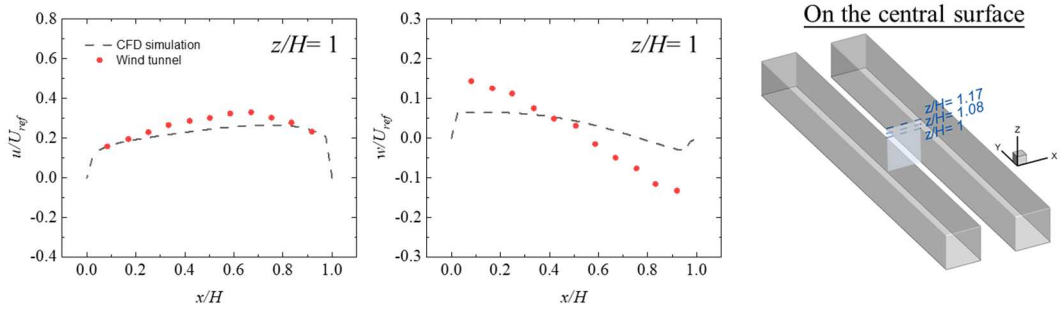

(b)

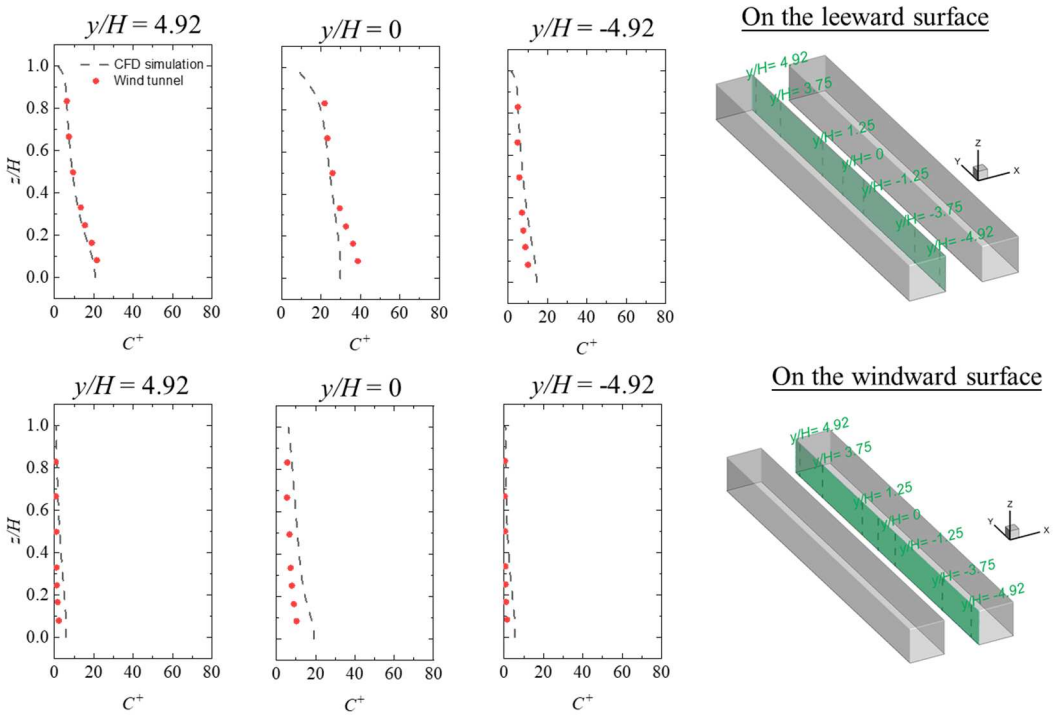

(c)

Figure 4 Comparison of WT results and the simulated (a) u/U_{ref} and v/U_{ref} the along a horizontal line on the vertical corner plane, (b) u/U_{ref} and w/U_{ref} along a horizontal line on the vertical central plane, and (c) C^+ along three vertical lines on the leeward and windward building surfaces

5. Results and discussion

5.1 Influence of traffic movement above different sides

When the TTFs occur, there are non-uniform pollutant emissions and TPFT on both sides of the street. The influence of non-uniform pollutant emissions has been discussed by our previous studies (Li et al., 2020; Ming et al., 2018). It is found that due to the canyon vortex (main vortex), the leeward-congestion TTFs have a higher leeward concentration than the windward-congestion TTFs with the same volume. For further comparison, Appendix A1 for illustrating the influence of non-uniform pollutant emission is supplemented. Prior to investigation on the TTFs, this section attempts to investigate the second characteristic of TTFs (non-uniform TPFT). Therefore, it is important to find out how different-side traffic motion affects pollutant dispersion.

5.1.1 Influence of traffic movement on mean flow and TKE

For the one-way traffic flow, it is observed that the each-side traffic movement has a minor influence on the flow structure and the vertical wind velocity (Figure 5 (b) & (c)) as well as the streamwise wind velocity (Figure A3 (b) & (c)) at the vertical cross-sections. However, the flow structure and corresponding spanwise velocity at the pedestrian level significantly change with the traffic movement on the different sides (Figure 5 (b) & (c)). At the horizontal cross-section (i.e., the pedestrian level (1/12 *H* above the ground)), the leeward traffic flow going along the direction of +y leads to a leeward channeling flow from right to left with stronger ventilation. The windward traffic flow also alters the direction of airflow, which turns to the direction of windward traffic flow (the direction of -y). Nonetheless, the windward traffic flow does not produce the channeling flow inside the street canyon (Figure 5 (b) & (c)). Besides, each side traffic movement strengthens the corner vortex at the lateral entrance of this traffic flow. For example, there is a stronger corner vortex close to the right lateral entrainment for leeward traffic movement. For a two-way traffic flow with the same condition, the channeling flows still appear above both side traffic lanes (Figure 5 (d)). It should be noted that the leeward channeling flow becomes weaker due to the influence of windward traffic movement. Besides, the positive effect of a one-way traffic flow on lateral ventilation set off each other.

Besides stronger ventilation caused by the traffic movement, there is a stronger TKE around the traffic lanes (Figure 6). These phenomena result from the composite effect of two influential aspects. One is that the traffic movement induces the TKE produced at the lateral boundary along the traffic lanes. The other is that the interaction of traffic movement and airflow modifies the mean flow motion into wake turbulence, which leads to the production of TKE as a result. It should be noted that the enhancement of TKE is only limited to the vicinity of traffic lanes, at either the vertical cross-sections or the horizontal cross-section. For instance, the windward traffic movement only causes a stronger TKE level at the windward side (Figure 6(c)).

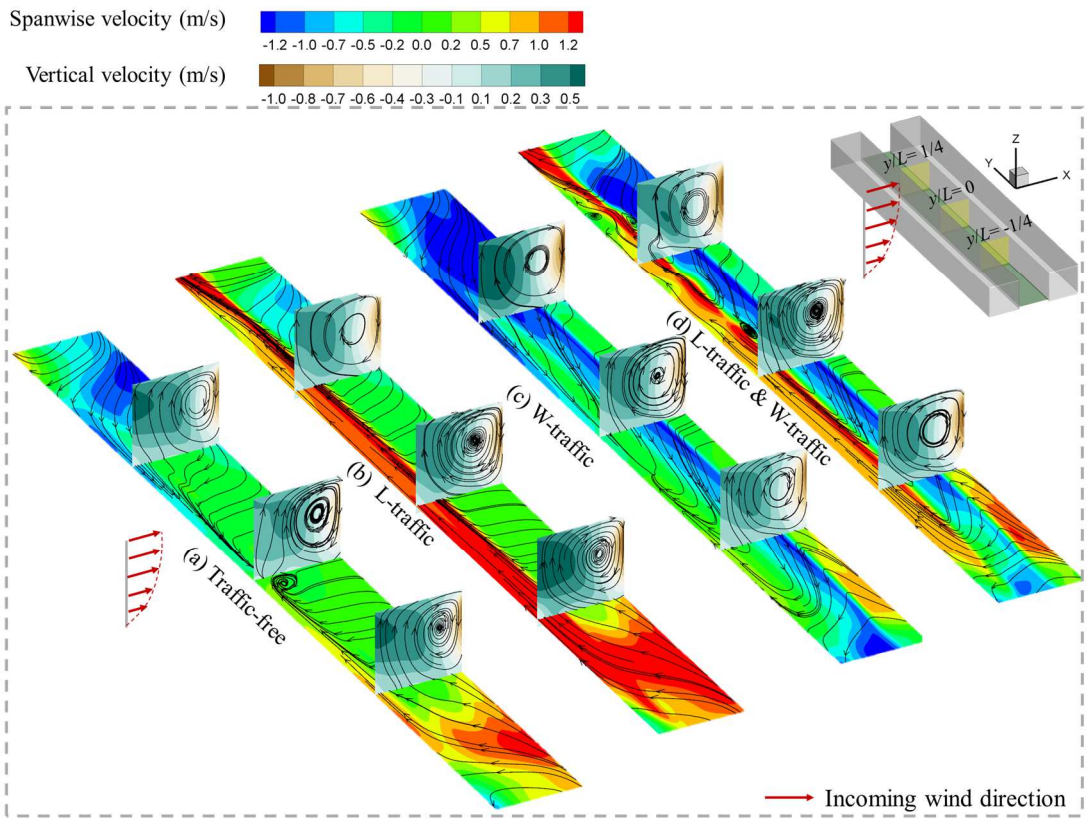

Figure 5 Predicted spanwise wind velocity at the pedestrian level and the vertical wind velocity on the vertical cross-sections for (a) traffic-free case, (b) leeward traffic flow (L-traffic) case, (c) windward traffic flow (W-traffic) case, and (d) L-traffic & W-traffic

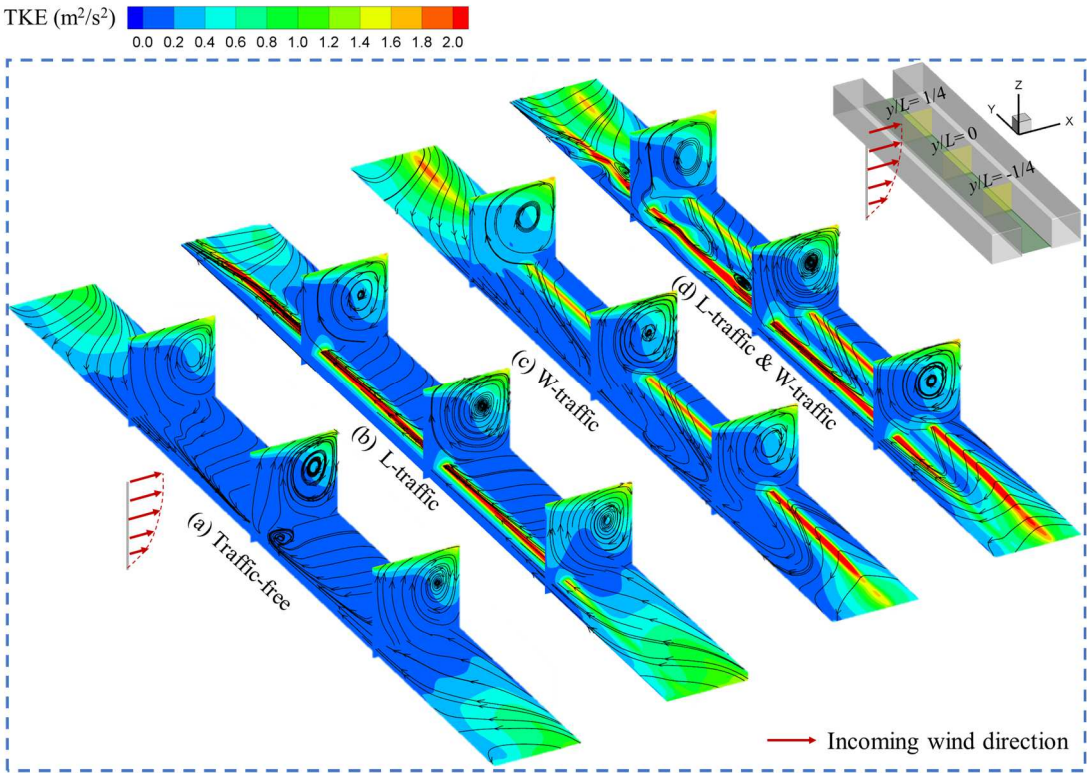

Figure 6 Predicted TKE at the pedestrian level and on the vertical cross-sections for (a) traffic-free case, (b) L-traffic case, (c) W-traffic case, and (d) L-traffic & W-traffic

5.1.2 Influence of traffic movement on pollutant dispersion

For the traffic-free case, due to the canyon vortex (main vortex) at the vertical cross-section, the pollutants tend to accumulate at the leeward side. Thus, there is a stronger leeward pollutant concentration (Figure 7(a) and Figure 8). Besides, the corner vortex causes the inward airflow at the pedestrian level from the lateral boundary, which results in a stronger concentration close to the symmetry plane (Figure 7(a) and Figure 8).

When the influence of one-way traffic movement is considered, there is still a higher pollutant concentration at the leeward side (Figure 7(b) & (c)). Nonetheless, there are some marked changes in the distribution of pollutants within the street canyon, especially at the leeward pedestrian level. First, as seen in Figure 7(b) & (c)), each side traffic movement pushes pollutants to the "downstream" position of traffic flow at the leeward side (Figure A4 illustrates the traffic flow "downstream"). As shown in Figure 8(a), the position of maximum pollutant concentration at the leeward side shifts to the

traffic flow "downstream". For instance, the leeward traffic movement (from right to left) result in a higher leeward pollutant concentration on the left side (Figure 7(b)). Second, the leeward traffic movement causes a lower leeward concentration than the windward traffic movement (Figure 7(b) & (c)). Besides, leeward traffic movement even leads to a reduction in maximum leeward concentration (about 8%), when compared with the traffic-free case. In contrast, the windward traffic movement almost does not reduce the maximum leeward concentration. The possible reason is the stronger leeward TKE induced by the traffic movement. Third, each-side traffic movement greatly reduces the maximum windward pollutant concentration (about 30% –32%), compared to the traffic-tree case (Figure 7(a)–(c)). Like the distribution of leeward pollutants, the position of maximum windward pollutant concentration also shifts to the traffic flow "downstream" (Figure 8(b)). Differently, the windward traffic movement does not cause a lower windward concentration than the leeward traffic movement.

For the two-way traffic flow, the traffic movement dilutes the significant accumulation of pollutants at the center region of the leeward side, compared to the traffic-free case (Figure 7(d)). Therefore, the maximum leeward pollutant concentration decreases (Figure 8(a)). Nevertheless, the two-way traffic movement causes a higher pollutant concentration close to the lateral boundary (Figure 8(a)). Besides, the position of maximum leeward pollutant concentration shifts to the direction of leeward traffic movement (+y). It is because that the leeward traffic movement plays a more important role in the re-distribution of leeward pollutants. On the windward side, pollutant concentration basically decreases, compared to the traffic-free case. Unlike the leeward side, the windward pollutant concentration still stays symmetric (Figure 8(b)).

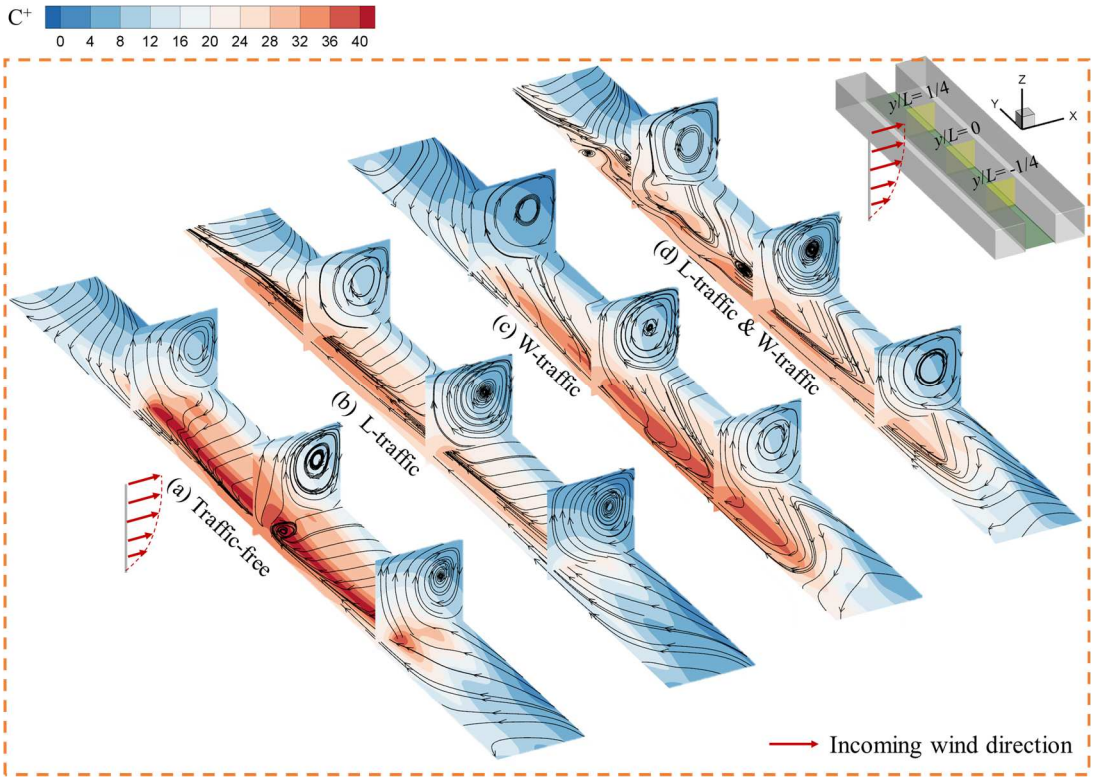

Figure 7 Predicted C^+ at the pedestrian level and on the vertical cross-sections for (a) traffic-free case, (b) L-traffic case, (c) W-traffic case, and (d) L-traffic & W-traffic case

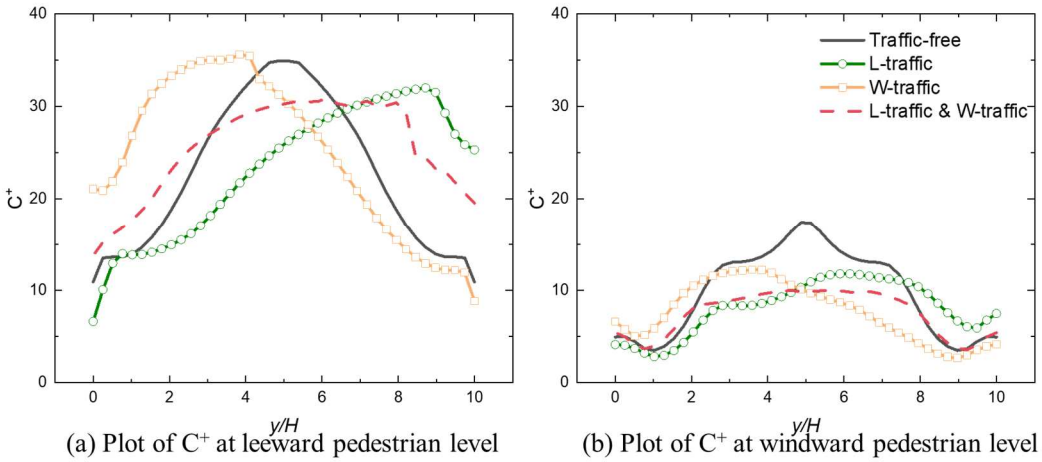

(a) Plot of C^+ at leeward pedestrian level (b) Plot of C^+ at windward pedestrian level

Figure 8 Horizontal profile of C^+ along with the (a) leeward pedestrian level and (b) windward pedestrian level. Herein, the location to record the horizontal distribution of C^+ is 10 mm away from the two-side building surface.

For a better understanding of the influence of the traffic movement on the in-canyon pollutant distribution, it is necessary to conduct a budget analysis to estimate the contribution of advection and turbulent diffusion for pollutant transport (Li et al.,

2009). The magnitudes of the advection term and turbulent diffusion term can be calculated by $-U_j\partial[C^+]/\partial x_j$ (1/s) and $\partial/\partial x_j(-\frac{D_t\partial[C^+]}{\partial x_j})$ (1/s), respectively (Baik et al., 2007; Weerasuriya et al., 2022). It should be noted that the negative value of either advection or turbulent diffusion terms is responsible for transporting pollutants away from this position. In contrast, the positive values mean these terms make the pollutant gather there (Li et al., 2009).

Figure 9 shows the spatial distribution of advection and turbulent diffusion term at the pedestrian level and on the vertical cross-sections. First, no matter for one-way or two-way traffic movements, there is a more significant change in the distribution of turbulent diffusion terms compared to the traffic-free case (Figure 9 (e)–(h)). Their influence on the distribution of advection terms is minor (Figure 9 (a)–(d)). It means turbulent diffusion caused by traffic movement plays a more critical role in dispersing pollutants. Second, the streamlines (from the lateral boundary to the street center at the leeward side in the traffic-free case) are significantly altered by traffic movement (especially for the leeward traffic movement). For the case of leeward traffic, the leeward streamlines are in line with the traffic movement direction. Although the traffic movement doe not significantly increase the intensity of advection terms, the negative value of unidirectional advection terms (from "upstream of traffic flow" to "downstream of traffic flow") means the traffic movement will push the pollutants downstream along the traffic direction. This finding can explain why each side's traffic movement moves pollutants to the "downstream" position of traffic flow at the leeward side. Third, pollutant turbulent diffusion terms are consistent with the distribution of TKE. In other words, the leeward traffic has a more significant negative value in the vicinity of the leeward pedestrian level. This stronger turbulent diffusion term is responsible for the reduction of maximum leeward concentration when compared to the windward traffic movement (observed above).

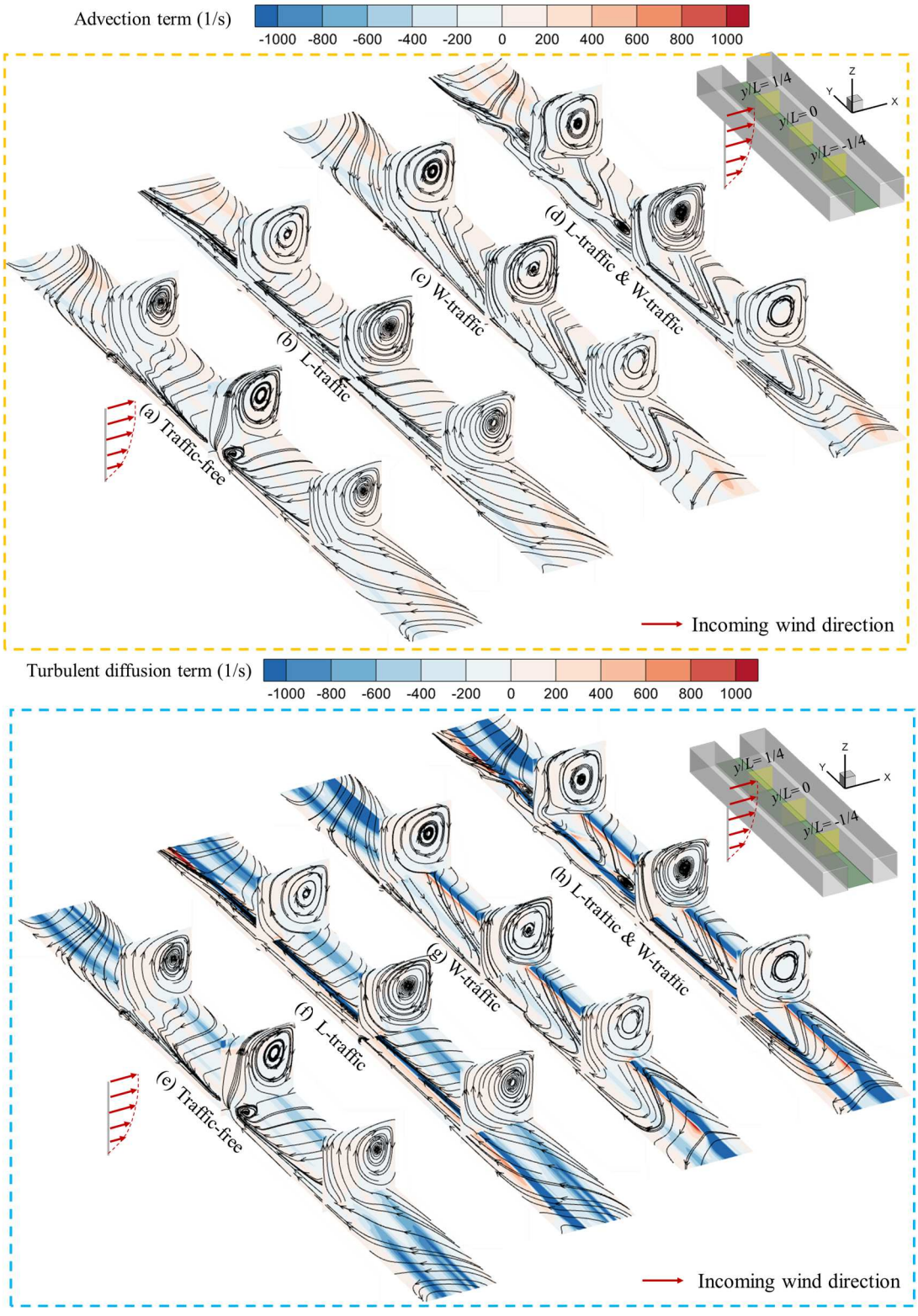

Figure 9 Budget analysis at the pedestrian level and on the vertical cross-sections

5.2 Studies on traffic tidal flow

This section attempts to mimic the real pollutant distribution when the TTFs occur. Accordingly, the influence of non-uniform pollutant emission and non-uniform TPFT

are simultaneously considered. As discussed above, there is a higher pollutant emission at the leeward/windward side while a stronger TPTF at the windward/leeward side for the TTF with leeward/windward congestion. To include more actual scenarios as much as possible when the TTFs occur, another three impact factors are also considered, i.e., the building separation, the canyon aspect ratio, and the incoming wind direction.

5.2.1 Base case

For the base case, the building geometry keeps in line with the WT (H/W = 1). The traffic simulating setting and corresponding pollutant source strength are adjusted according to the traffic condition of different TTFs observed. As discussed above, traffic movement significantly influences the distribution of spanwise velocity and TKE within the street canyon. Thus, these two parameters are chosen to evaluate how different TTFs affect the in-canyon mean flow and TKE.

Figure 10(a) shows that the TTF with leeward congestion remarkably changes the original streamlines on the windward side. Once the downward airflow at the windward side reaches the ground, almost turns towards the windward traffic flow "downstream" (right side). This is because there is stronger windward traffic movement. Meanwhile, the airflow towards the leeward traffic flow "downstream" is mildly enhanced due to the leeward traffic movement. Similarly, the TTF with windward congestion results in a more significant channeling flow in the vicinity of the leeward building surface. However, the windward congested traffic flow does not greatly change the flow structure close to the windward surface. For both TTFs, a significant enhancement of TKE is observed above the non-congestion side (Figure 10(b)). As seen in Figures 10(e) and (f), it is observed that turbulent diffusion plays a more critical role in the pollutant distribution inside the street canyon.

As discussed in Appendix A2, if only the non-uniform pollutant emission is considered, the leeward-congestion TTF will have a higher leeward concentration than the windward-congestion TTF. Its average/maximum leeward concentrations are about 14% and 12% higher. The windward-congestion TTF results in a higher windward

concentration. Its average/maximum windward concentrations are about 44% and 41% higher. A similar conclusion could still be drawn when the non-uniform pollutant emission and TPFT are simultaneously simulated. In terms of two-side average or maximum pedestrian-level concentration, the TTF with leeward congestion still causes a higher leeward concentration (13% and 10% for average and maximum value), while the windward-congestion TTF results in a higher windward concentration (49% and 44% for average and maximum value) (Table 1). Differently, due to the leeward traffic movement, the position of maximum leeward pollutant concentration shifts toward the leeward traffic flow "downstream", especially for the TTF with windward congestion (Figure 10 (c)&(d)). This is because the TTF with windward congestion leads to unidirectional advection terms along the traffic direction close to the leeward building surface. As a result, at the left side of the leeward pedestrian level (leeward traffic flow "downstream"), the windward-congestion TTF has a higher concentration (Figure 10 (d)). For the windward pedestrian level, the pollutant concentration distribution remains basically symmetric. When comparing Table 1 and Table A1, the non-uniform TPFT slightly decreases the difference of pollutant concentration at the leeward side caused by the non-uniform pollutant emission but increases this concentration difference at the windward side.

Moreover, the area-average pollutant concentration of the entire pedestrian level (C^+_{ped}) and the volume-average pollutant concentration of the whole street canyon (C^+_{canyon}) are compared for different TTFs with different-side congestion. It is found that the TTF with windward congestion causes a higher C^+_{ped} (Table 1). It should be attributed to a weaker turbulent diffusion on the windward side (Figure 10(f)), while a stronger pollutant emission exists on this side. Thus, these massive pollutants from the windward emission source tend to accumulate at the pedestrian level, especially at the center of the street (Figure 10(c)). On the other hand, Figures 10 (e) and (f) show that these two TTFs have a similar ability to transport pollutants upwards in the vicinity of the leeward surface by advection and turbulent diffusion terms on the vertical sections.

In other words, a similar proportion of pollutants are transported away from their previous position upwards. The leeward-congestion TTF, which has a stronger leeward emission, naturally has more pollutants away from the pedestrian level (Figure 10(c)). As a result, there is a higher C^{+}_{ped} for the windward-congestion TTF.

As Li et al. (Li et al., 2009), turbulent diffusion terms dominate the pollutant removal across the roof level. However, the variations of TTFs do not significantly change the distribution of turbulent diffusion terms at the roof level (Figure 10(f)). Thus, more pollutants escape across the roof level for the leeward-congestion TTF since there are more pollutants away from the pedestrian level. At the same time, the difference in advection or turbulent diffusion terms caused by different TTFs is also minor at the lateral entrance (Figure 10(e) and (f)). Consequently, the windward-congestion TTF also results in a higher C^{+}_{canyon}.

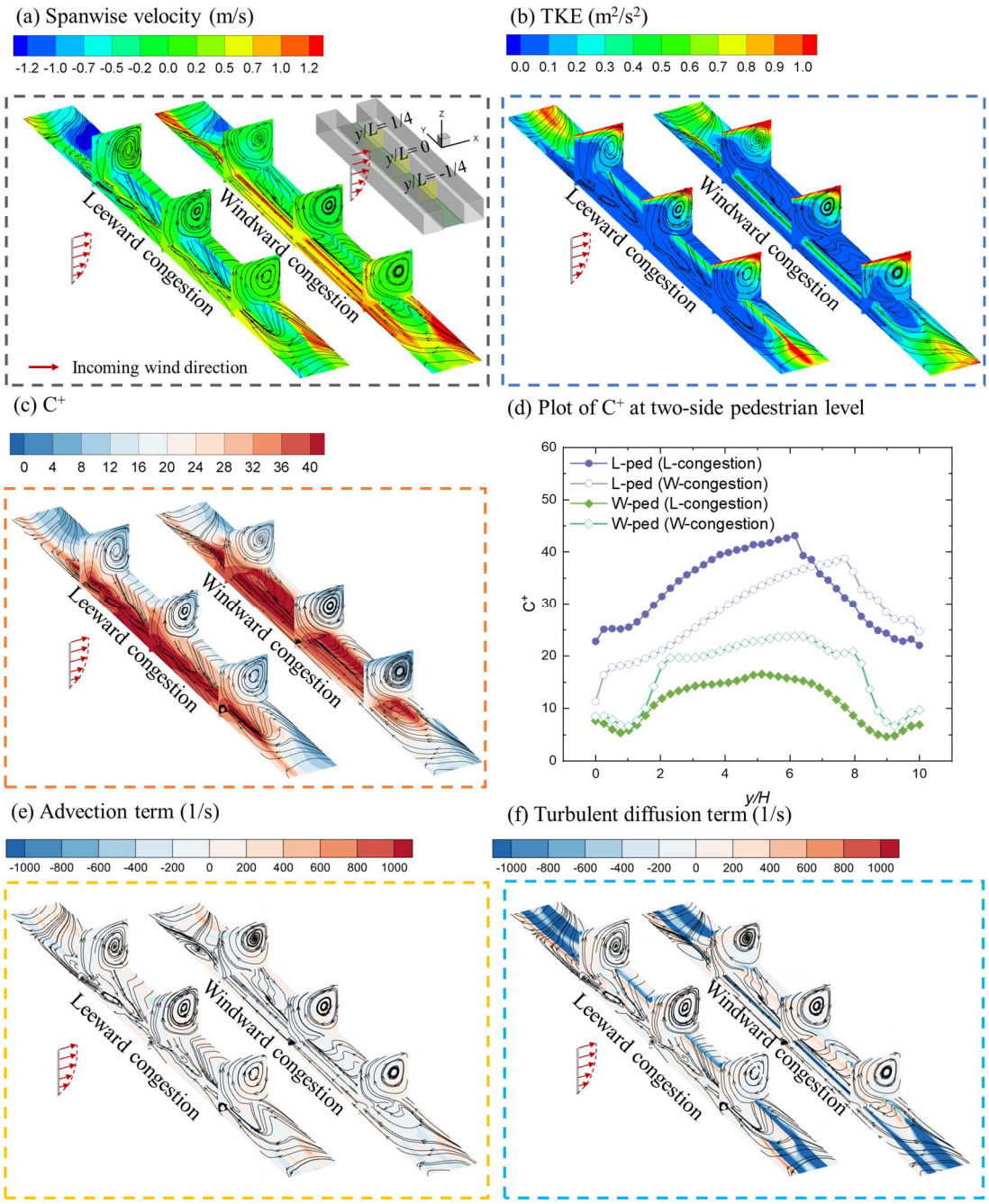

Figure 10 Predicted (a) spanwise wind velocity, (b) TKE, (c) C^+ at the pedestrian level and on the vertical cross-sections, (d) plot of C^+ at two-side pedestrian level (The location to record the horizontal distribution of C^+ is also 10 mm away from the two-side building surface), (e) advection term, and (f) turbulent diffusion terms at the pedestrian level and on the vertical cross-sections under the leeward and windward congestion TTFs for the base case.

Table 1 C^+ difference between L- & W- congestion TTFs for the base case

	Average C^+_{Lee}	Average C^+_{Win}	Maximum C^+_{Lee}	Maximum C^+_{Win}	Average C^+_{ped}	Average C^+_{canyon}
L-congestion	32.6	11.2	43.1	16.5	25.5	17.4
W-congestion	28.3	16.7	38.8	23.8	29.1	18.4
C^+ difference between *L*- & *W*- congestion (%)	13%	-49%	10%	-44%	-14%	-6%

C^+_{Lee} and C^+_{Win} are the pollutant concentration along the leeward and windward pedestrian level; C^+_{ped} is the area-average pollutant concentration of the entire pedestrian level; C^+_{canyon} is the volume-average pollutant concentration of the whole street canyon.

5.2.2 Effects of building separation

In the base case, all buildings are assumed to be closely packed together without any separation between buildings. In effect, the building separation is often observed, which is directly related to the permeability of incoming wind (Li et al., 2021a; Ng and Chau, 2014). The building separation is defined as the percentage of the length of building separation *S* to the length of canyon *L* (Ng and Chau, 2014). Herein, the separation of 10% permeability is considered.

As seen in Figure 11(a), there is a marked jet flow because of the building separation. These jet-flows cut off the channeling flow induced by the traffic movement. Accordingly, it is not easy to transport the pollutant along the leeward side on a large scale anymore. Due to the building separation, the TKE level at the bottom of the street canyon is much higher compared to the base case. The enhancement of TKE induced by the traffic movement becomes insignificant (Figure 11 (b)). As a result, the change in the distribution of turbulent diffusion terms caused by different TTFs becomes less evident (Figure 11(f)). The influence of non-uniform TPFT reduces and the forced convection dominates the distribution of pollutants within the street canyon. Therefore, there is still a higher leeward concentration for the leeward-congestion TTF. At the windward side, the windward-congestion TTF leads to a higher concentration (Figure 11 (c) & (d)). When comparing the baseline case and the building separation case, it is

found that the difference of pollutant concentration caused by non-uniform pollutant emission decreases at the leeward side but increases at the windward side (Table 1 & Table 2). Table 2 also shows that there is still higher C^{+}_{ped} and C^{+}_{canyon} for the windward-congestion TTF. Compared to the base case, the difference of either C^{+}_{ped} or C^{+}_{canyon} due to different TTFs also becomes smaller (Table 1 & Table 2). It could be attributed to the higher windward turbulent diffusion term for the windward-congestion TTF when compared to the base case (Figure 10 (f) & Figure 11 (f)).

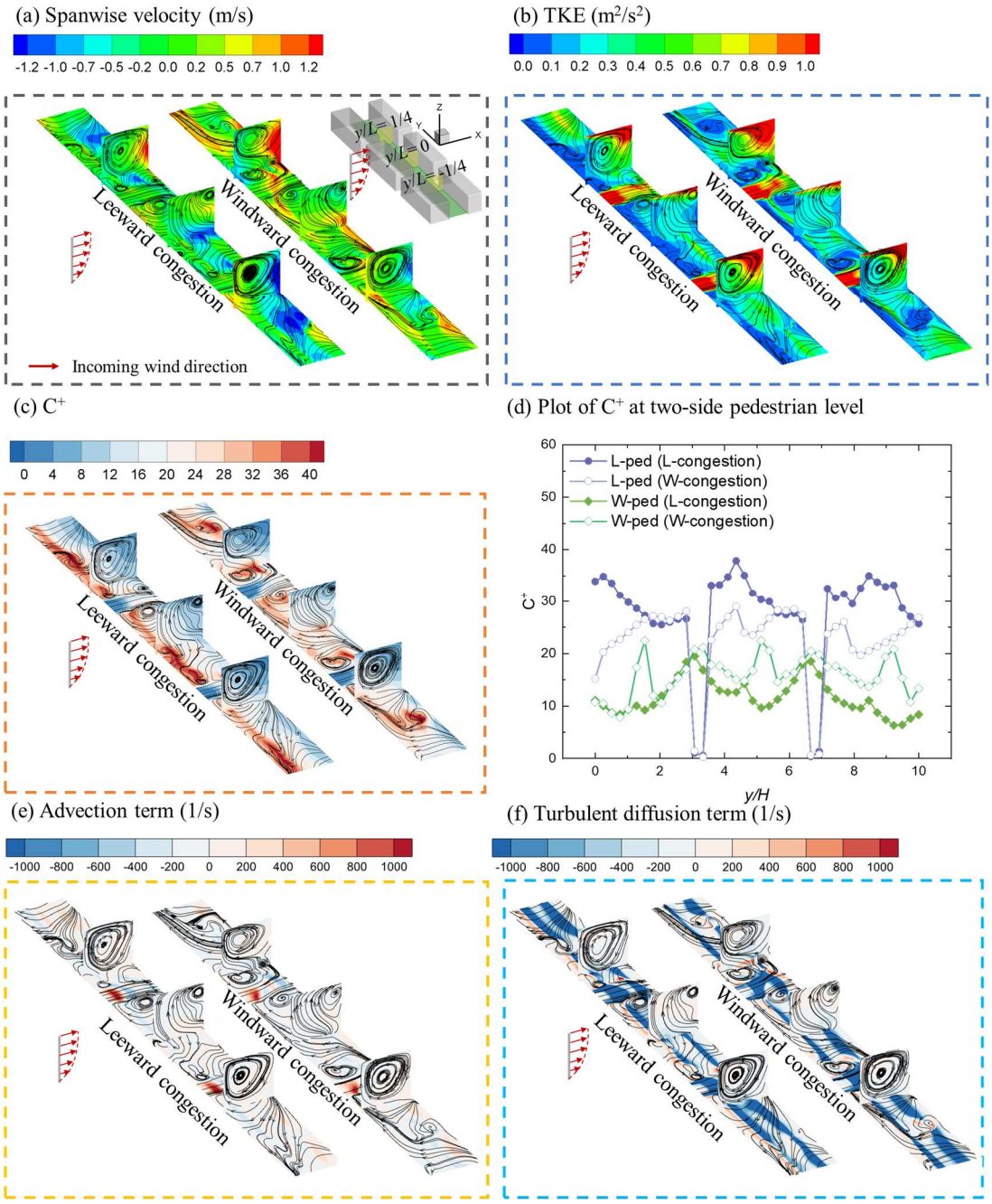

Figure 11 Same as Figure 10 but for the building separation

Table 2 C^+ difference between L- & W- congestion TTFs with the building separation

	Average C^+_{Lee}	Average C^+_{Win}	Maximum C^+_{Lee}	Maximum C^+_{Win}	Average C^+_{ped}	Average C^+_{canyon}
L-congestion	27.5	11.8	37.8	19.5	20.6	12.5
W-congestion	22.2	15.9	29.0	22.5	22.4	13.1
C^+ difference between *L*- & *W*- congestion (%)	19%	-35%	23%	-15%	-9%	-5%

5.2.3 Effects of street canyon aspect ratio

The regular street canyon (H/W= 1) is chosen as the base case. In fact, the street canyon varied with the canyon aspect ratio, H/W. Herein, the influence of TTFs is evaluated within a deep street canyon of H/W= 2 for comparison. Our previous study shows stronger lateral entrainment from the side boundary in a deeper street canyon (Li et al., 2021b). With stronger lateral entrainment, the channeling flow induced by the traffic movement could be enhanced.

As seen in Figure 12(a), the influence of traffic movement indeed becomes more significant. Compared to the regular street canyon, the combined effect of stronger lateral entrainment and the windward traffic movement (for the leeward-congestion TTF) also causes a channeling flow. It will shift the position of maximum windward concentration. Like the regular street canyon, there still is channeling flow for the windward-congestion TTF. Thus, in terms of horizontal distribution of pollutants, each TTF results in a symmetric distribution of pollutant concentration close to the congestion-side, while an asymmetric pollutant distribution on the opposite side (Figure 12(c) and (d)). Besides, compared to the regular street canyon, the traffic movement causes a larger improvement of TKE, which contributes to the dispersion of pollutants at the lower space of the street canyon (Figure 12(b)). As a result, the leeward-congestion TTF and the windward-congestion TTF have a similar maximum leeward or windward pollutant concentration (Figure 12(d) & Table 3), where the difference is

less than 6% or 7%. The leeward-congestion TTF causes a 12% higher leeward concentration. The windward-congestion TTF still has a 20% higher windward concentration (Table 3), much lower than that of the regular street canyon (49% shown in Table 1). The possible reason is that the turbulent diffusion term has a more significant negative value around the windward pollutant source inside the deep street canyon (Figure 12(f)) compared to the base case. Therefore, Table 3 also shows that the difference of C^{+}_{ped} reduces to almost 4% in this deep street canyon. However, the difference of C^{+}_{ped} is about 14% in the baseline case. Similarly, there is a minor difference of C^{+}_{canyon} inside the deep street canyon.

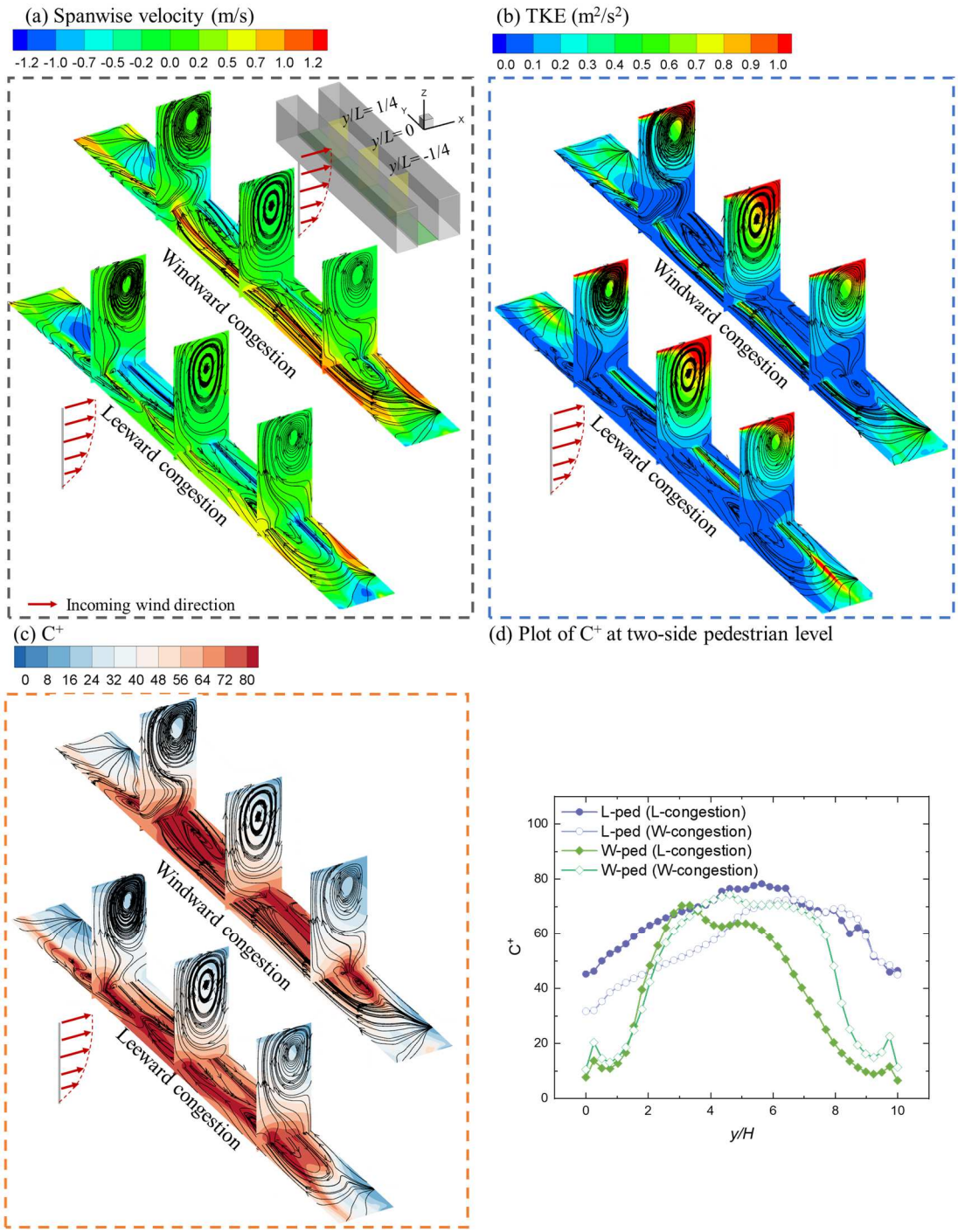
(a) Spanwise velocity (m/s)
-1.2 -1.0 -0.7 -0.5 -0.2 0.0 0.2 0.5 0.7 1.0 1.2
(b) TKE (m²/s²)
0.0 0.1 0.2 0.3 0.4 0.5 0.6 0.7 0.8 0.9 1.0
y/L= 1/4
y/L= 0
y/L= -1/4
Windward congestion
Leeward congestion
Incoming wind direction
(c) C⁺
0 8 16 24 32 40 48 56 64 72 80
(d) Plot of C⁺ at two-side pedestrian level
L-ped (L-congestion)
L-ped (W-congestion)
W-ped (L-congestion)
W-ped (W-congestion)
C⁺
y/H

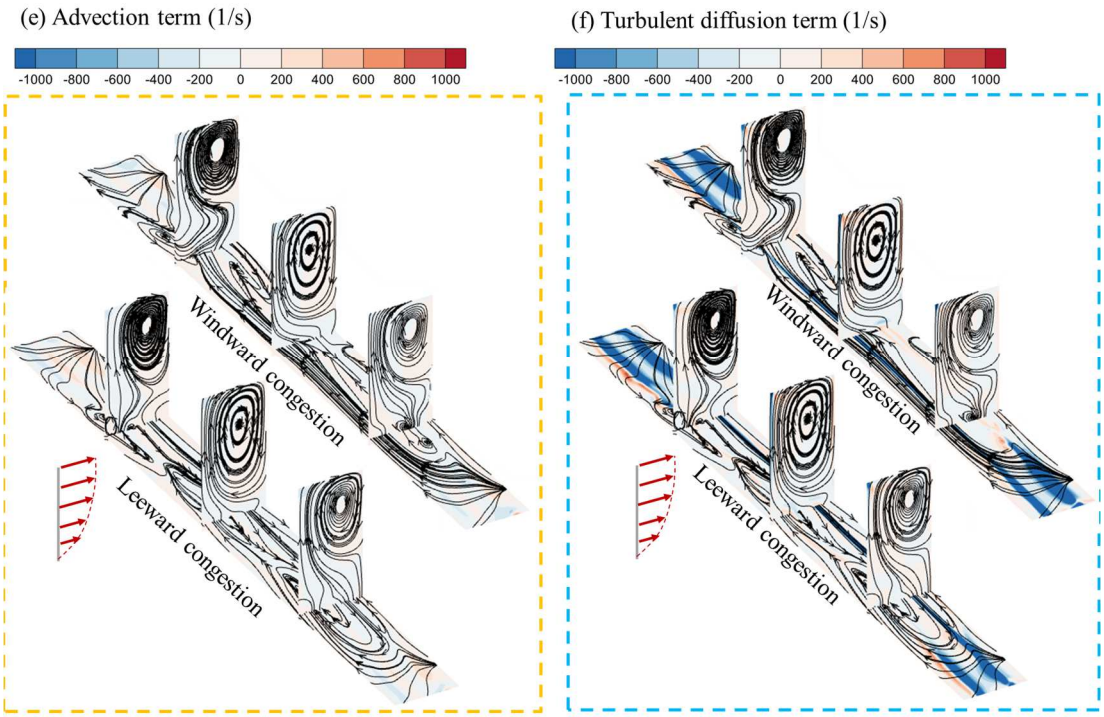

Figure 12 Same as Figure 10 but for the deep street canyon

Table 3 C^+ difference between L- & W- congestion TTFs for the deep street canyon

	Average C^+_{Lee}	Average C^+_{Win}	Maximum C^+_{Lee}	Maximum C^+_{Win}	Average C^+_{ped}	Average C^+_{canyon}
L-congestion	64.6	38.4	78.3	70.4	29.7	16.2
W-congestion	56.6	46.2	72.5	74.5	31.0	16.6
C^+ difference between *L*- & *W*- congestion (%)	12%	-20%	7%	-6%	-4%	-2%

5.2.4 Effects of incoming wind direction

The perpendicular wind is considered in the base case. In effect, the incoming wind varies with various wind directions. Therefore, this section attempts to explore the influence of TTF under a parallel wind. Unlike the perpendicular wind, we can only intuitively define two-side traffic flow, i.e., the right-congestion and left-congestion TTFs. For this two-way traffic, the right traffic flow goes along the wind direction while the left traffic flow goes against the wind direction (Figure A5). Therefore, the right-congestion TTF has a stronger traffic movement against the incoming wind.

As shown in Figure 13(a), both TTFs do not significantly affect the flow structure at the pedestrian level. The pedestrian-level streamlines are almost from the upstream entrance to the downstream outlet of the street canyon. This is because, unlike the perpendicular wind, the in-canyon airflow induced by the parallel wind is strong enough. Thus, the parallel-approaching wind almost dominates the distribution of pollutants. Along the incoming wind direction, both advection and turbulent diffusion have negative values at the bottom of the street canyon, which pushes the pollutants downstream. Accordingly, the trend of pollutant distribution along the two-side pedestrian level is consistent. For both TTFs, their two-side concentration significantly increases at the entrance section and then only changes slightly downstream (Figure 13(c) & (d)). Nonetheless, the left-/right- congestion TTF still causes a higher left-/right- side concentration in terms of either average or maximum pollutant concentration (Table 4). This is because the horizontal turbulent diffusion (y+ direction) nearby the pollutant source contributes to the accumulation of pollutants above both-side pedestrian levels (Figure 13(f)). Besides, Table 4 presents that the TTF with congestion traffic goes along with the incoming wind direction (TTF with right congestion here), causing a lower C^{+}_{ped} or C^{+}_{canyon}. This is due to the significant enhancement of TKE on another side (left side) and also improves the TKE level on this side (right side) (Figure 13(b)). Thus, the right-side turbulent diffusion significantly increases to dilute the massive pollutant emission caused by the congestion (Figure 13(f)). In contrast, the stronger TPTF on the right side (its traffic direction is in line with the incoming wind direction) has little effect on the left-side turbulent diffusion for the TTF with left-side congestion (Figure 13(f)).

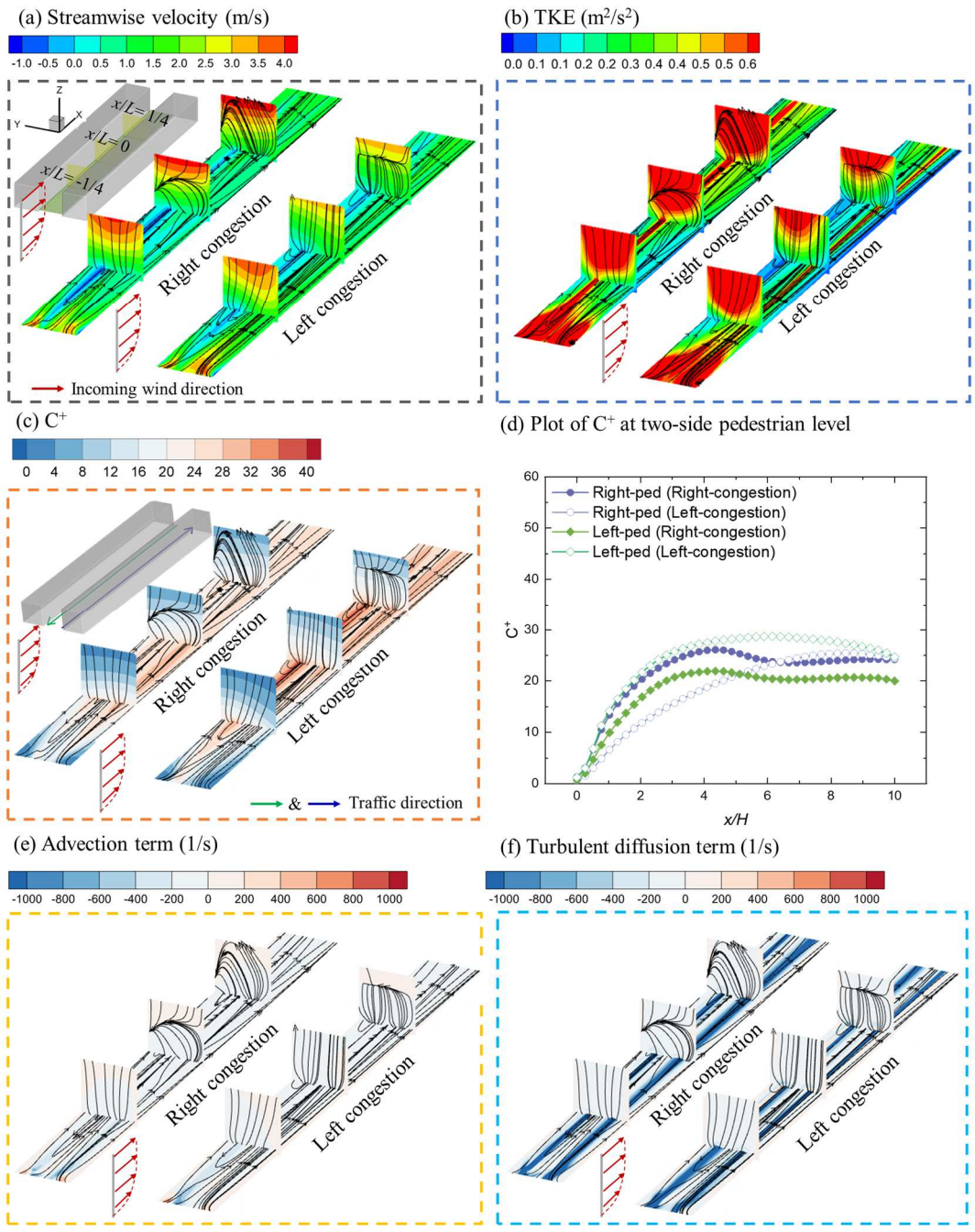

Figure 13 Same as Figure 10 but under a parallel wind

Table 4 C^+ difference between L- & R- congestion TTFs under a parallel wind

	Average C^+_{Lee}	Average C^+_{Win}	Maximum C^+_{Lee}	Maximum C^+_{Win}	Average C^+_{ped}	Average C^+_{canyon}
L-congestion	21.5	18.1	26.1	21.9	24.5	13.6
R-congestion	18.3	23.9	25.4	28.7	22.6	12.6
C^+ difference between *L*- & *R*- congestion (%)	15%	-32%	3%	-31%	8%	8%

6. Conclusion

This paper has presented numerical simulations with Computational Fluid Dynamics (CFD) to investigate the influence of traffic tidal flows (TTFs) on the in-canyon pollutant distribution. One of the characteristics of the TTFs, the influence of non-uniform traffic emission has been discussed in the literature. This study first attempts to explore the other of the characteristics of the TTFs, i.e., the non-uniform traffic-produced flow and turbulence (TPFT). Thus, the potential contribution of the leeward and windward TPFT is investigated to find out how different-side traffic motion affects pollutant dispersion. Second, this study simultaneously considers the non-uniform pollutant emission and non-uniform TPFT induced by TTFs, which are recorded by or previous observation. Finally, the influence of these TTFs is tested under different street canyon geometry and incoming wind condition. The major results are summarized as follows:

1) Both leeward and windward one-way traffic movement significantly impact the pedestrian-level flow structure. For example, the leeward TPFT causes a channeling flow along the leeward surface. They significantly affect the spanwise wind velocity and improve the TKE level around the traffic lanes but have a minor influence on the streamwise velocity. The budget analysis indicates turbulent diffusion terms play a more critical role in pollutant dispersion than the advection terms, considering the influence of TPFT. Besides, the unidirectional advection terms along the traffic direction make the pollutant away from the source and push them towards traffic flow "downstream".

2) If only the non-uniform pollutant emission is considered, the leeward/windward-congested TTF causes a higher average concentration on the leeward/windward side. Simultaneously considering the non-uniform pollutant emission and TPFT, both TTFs still cause a higher concentration close to the congested traffic lane. Differently, non-uniform TPFT significantly alters the spanwise distribution of concentrations at the

leeward side. The position of maximum leeward concentration shifts to the leeward traffic flow "downstream", especially for windward-congested TTF, while the distribution of windward concentration stays symmetric regardless of the TPFT.

3) When changing the building separation, building height, and incoming flow direction, TTFs still cause a higher concentration at the pedestrian level close to the congested traffic lane. This should be attributed to the horizontal turbulent diffusion terms around the pollutant source. Besides, the weaker windward turbulent diffusion for a windward-congestion TTF can not effectively remove the massive pollutant emission on this side. Thus, the TTF with windward congestion has a C^{+}_{ped} and C^{+}_{canyon}.

Based on the present study, the following suggestions are proposed for better air quality when the TTFs happen: 1) when the TTFs occur inside the urban street canyon, more attention should be paid to the pavements close to the congested traffic lanes. Green belts or solid barriers could be planted or installed between these traffic lanes and the pavements to mitigate the local accumulation of pollutants; 2) in terms of air quality of the whole street canyon, the TTF with windward congestion is worse. Hence, more optimization strategies to enhance the ventilation (e.g., keeping enough building separation or lift-up design) could be considered to mitigate the pollutant concentration.

In this research, the reduced-scale CFD simulation model is used to investigate the influence of traffic movement. The impact of TTFs is tested in a series of ideal street canyons to reduce the influence variables. As seen in Figure A6 taken by our previous study (Tidal phenomenon of urban road traffic occurred in a section of the street canyon in the 2nd Ring Road of Wuhan, China), the traffic tidal flow usually appears with the complicated street canyon structure. The influence of traffic tidal flow will be tested in the full-scale realistic street canyons in future work. Besides, the current *Re* number meets the reduced-scale model's independence requirement. However, Chew et al. (Chew et al., 2018) pointed out *Re* number for flow in a street canyon cannot be matched between reduced-scale experiments and full-scale field measurements. Also, Yang et al. (Yang et al., 2021) found that in some deep full-scale 2D canyons, this *Re* number

may reach 10^6–10^7. Thus, *Re*-independence tests are still necessary when the influence of traffic tidal flow in a full-scale model should be in future work.

Appendix

Appendix A1. Effects of non-uniform traffic emissions

Our previous studies have investigated the effects of non-uniform traffic emission (Li et al., 2020; Ming et al., 2018). Nonetheless, for comparison, this study still attempts to explore the non-uniform traffic emission under the same incoming condition and street canyon geometry. Herein, the setting of the non-uniform pollutant source stays consistent with the base case. However, the non-uniform TPFT of the base case is not included.

It's found that the leeward-congestion TTF has a higher leeward concentration than the windward-congestion TTF (Figure A1). Its average/maximum leeward concentrations are about 14% and 12% higher (Table A1). The windward-congestion TTF results in a higher windward concentration (Figure A1). Its average/maximum windward concentrations are about 44% and 41% higher (Table A1).

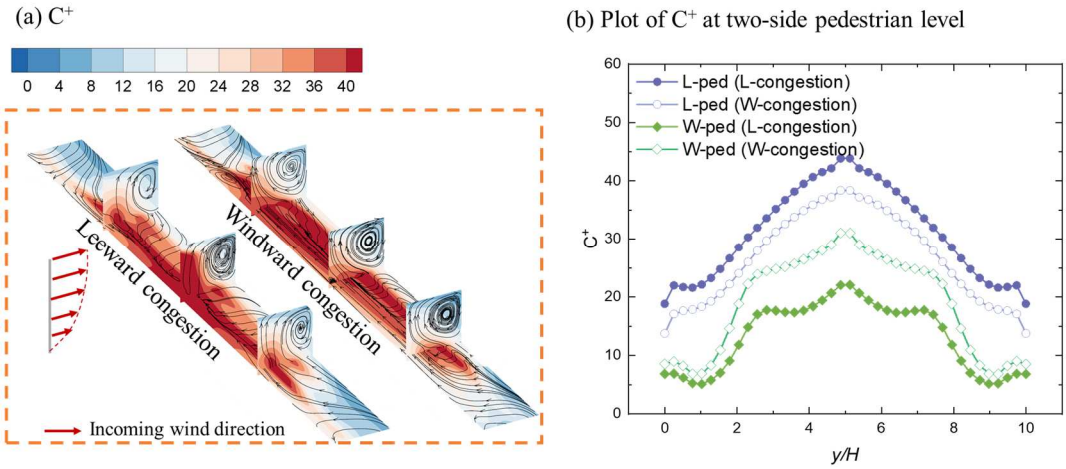

Figure A1 Predicted (a) C^+ at the pedestrian level and on the vertical cross-sections, and (b) plot of pedestrian-level C^+ for different non-uniform traffic emission

Table 1 C^+ difference between *L*- & *W*- congestion TTFs for different non-uniform traffic emissions

	Average C^+_{Lee}	Average C^+_{Win}	Maximum C^+_{Lee}	Maximum C^+_{Win}
L-congestion	31.2	13.2	43.8	16.5
W-congestion	26.8	19.0	38.4	23.8
C^+ difference between *L*- & *W*- congestion (%)	14%	-44%	12%	-41%

Appendix A2. Grid-sensitivity analysis

The grid-sensitivity analysis is performed against the WT. Figure A2 presents dimensionless streamwise and spanwise velocity components along three horizontal lines at the lateral plane and dimensionless pollutant concentrations on the leeward surface. The results show that those fine, basic, and coarse grids provide almost the same results of wind velocity and pollutant concentration, especially for the fine and basic. Furthermore, the grid-convergence index (GCI) proposed by Roache (Roache, 1997) is used to estimate the error of u/U_{ref} and v/U_{ref} on the basic grid.

$$GCI_u = F_s \left| \frac{r^p (u_{basic} - u_{fine}) / U_{ref}}{1 - r^p} \right| \quad (15)$$

$$GCI_v = F_s \left| \frac{r^p (v_{basic} - v_{fine}) / U_{ref}}{1 - r^p} \right| \quad (16)$$

where F_s is the safety factor taken as 1.25 when three or more grids are compared, r is the linear grid refinement (=2), p is the former order of accuracy (=2), u and v are streamwise and spanwise mean velocity in one of the two grids (basic and fine). The resulted average GCI_u and GCI_v for three horizontal lanes is 1.3% and 4.1%. By analyzing the discrepancy in wind speed and pollutant concentration of the three grids as well as comparing GCI values of the fine and basic grids, it can be concluded that the basic grid provides nearly grid-independent results, which can be further used for the remainder of this study.

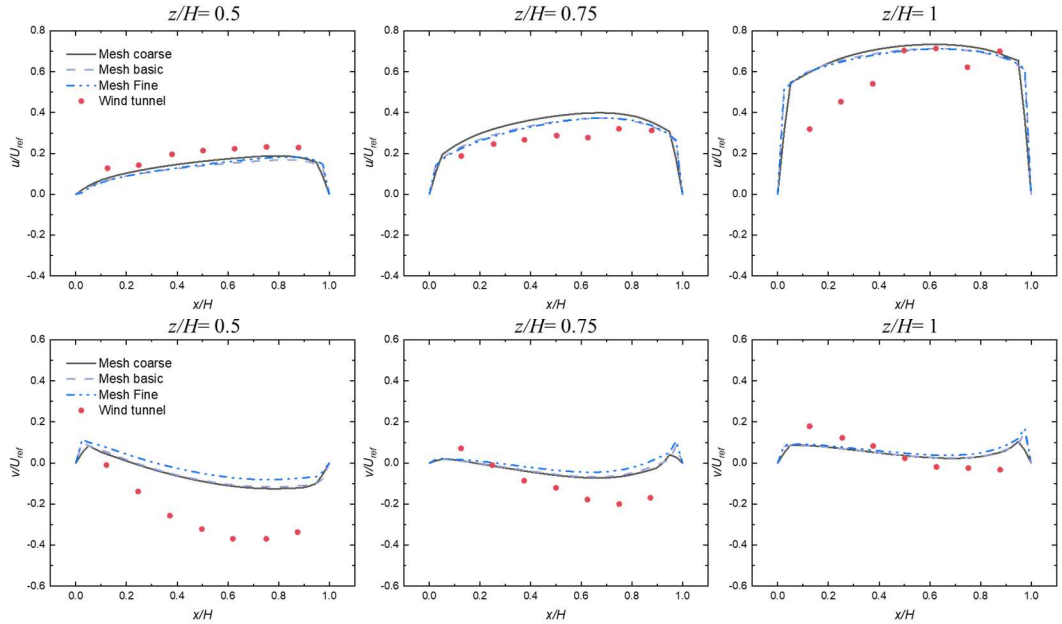

(a)

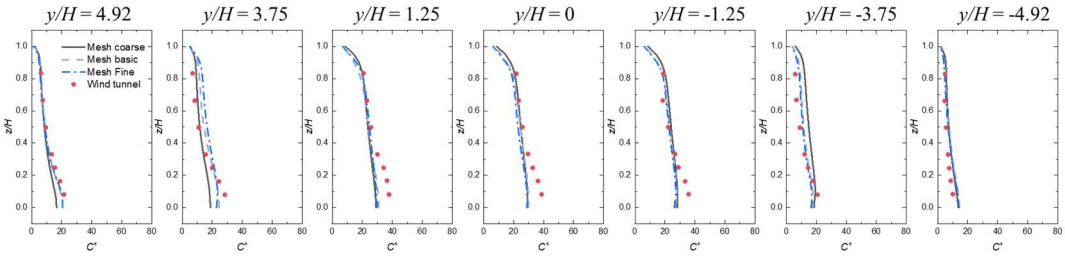

(b)

Figure A2 Comparison of dimensionless (a) streamwise mean velocity (u/U_{ref}) and spanwise mean velocity (v/U_{ref}) on the corner plane and (b) pollutant concentration C^+ on the leeward surface in coarse, basic, and fine grids

Appendix A3. Supplementary figures

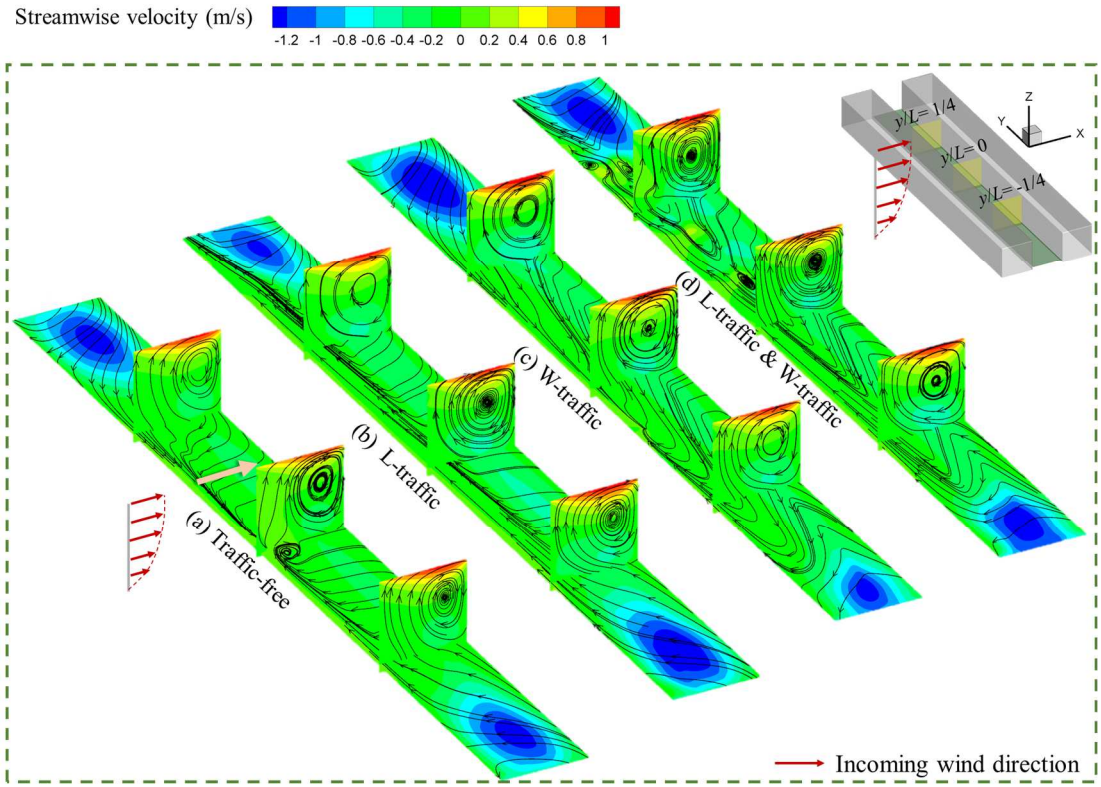

Figure A3 Predicted streamwise wind velocity at the pedestrian level and on the vertical cross-sections for (a) traffic-free case, (b) L-traffic case, (c) W-traffic case, and (d) L-traffic & W-traffic

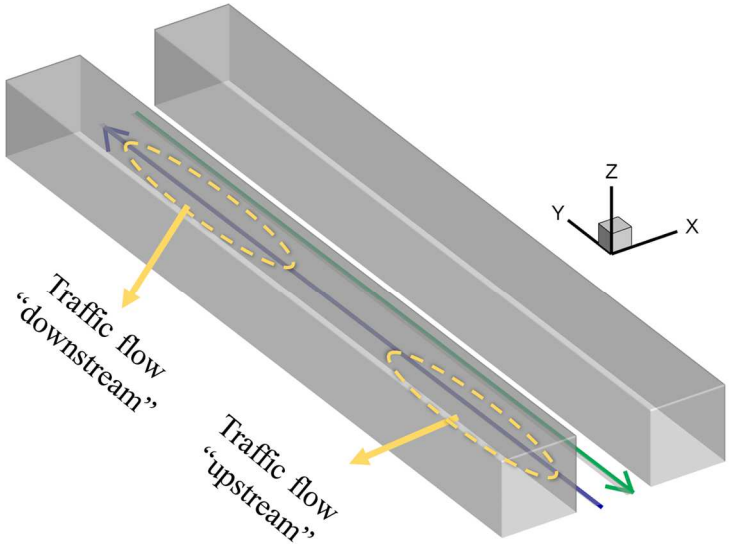

Figure A4 Illustration for traffic flow "upstream" and "downstream"

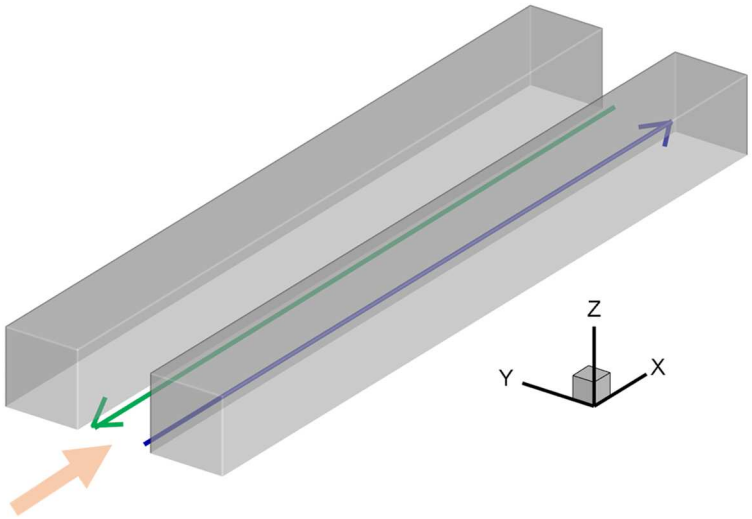

Figure A5 Illustration for the direction of both-side traffic flows under parallel incoming wind

Figure A6 Tidal phenomenon of urban road traffic (Photo was taken on Wednesday, 9 November 2016 at 7:23 a.m.) (Ming et al., 2018)

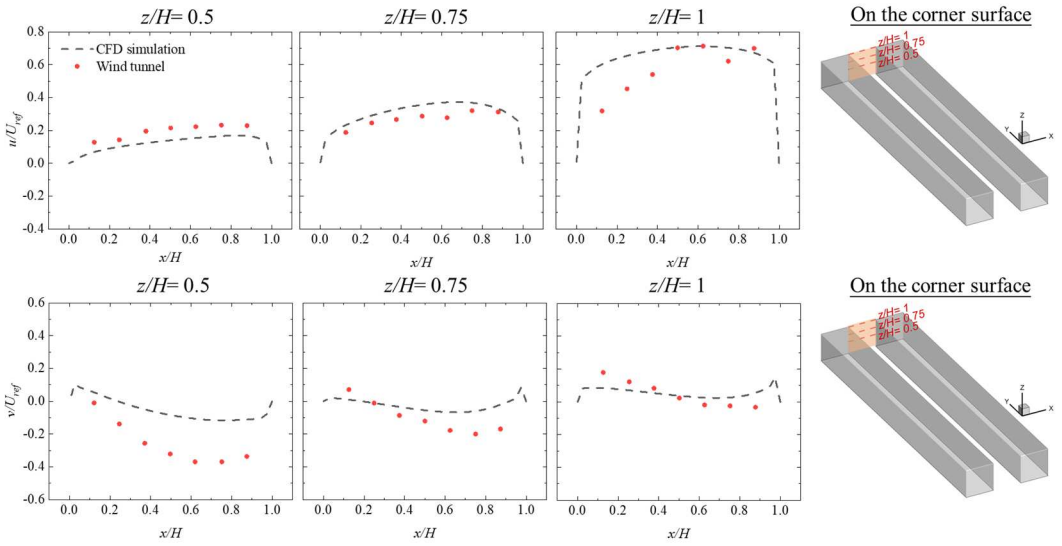
z/H= 0.5
z/H= 0.75
z/H= 1
On the corner surface
CFD simulation
Wind tunnel
u/U_ref
v/U_ref
x/H
z/H= 1
z/H= 0.75
z/H= 0.5

(a)

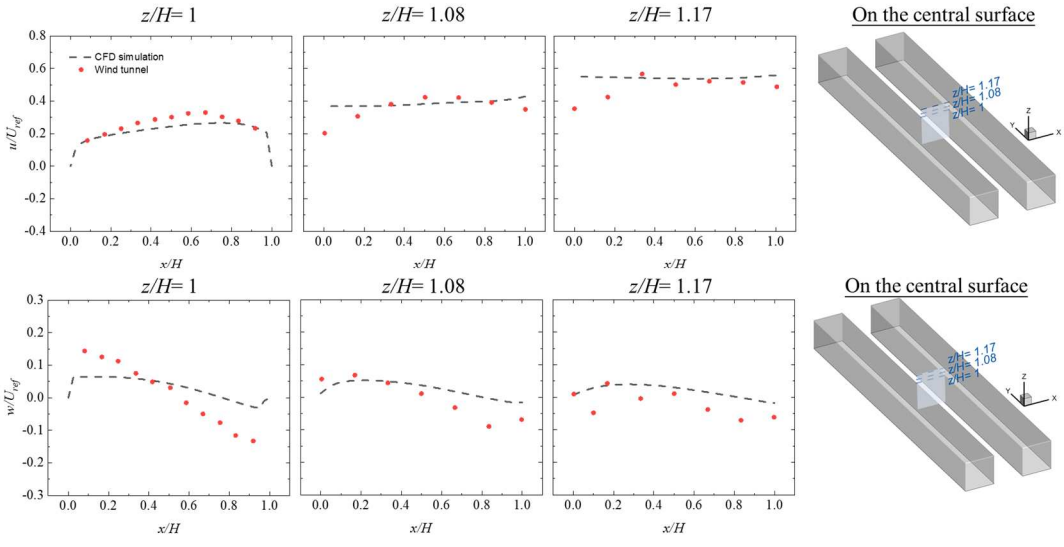
z/H= 1
z/H= 1.08
z/H= 1.17
On the central surface
CFD simulation
Wind tunnel
u/U_ref
w/U_ref
x/H
z/H= 1.17
z/H= 1.08
z/H= 1

(b)

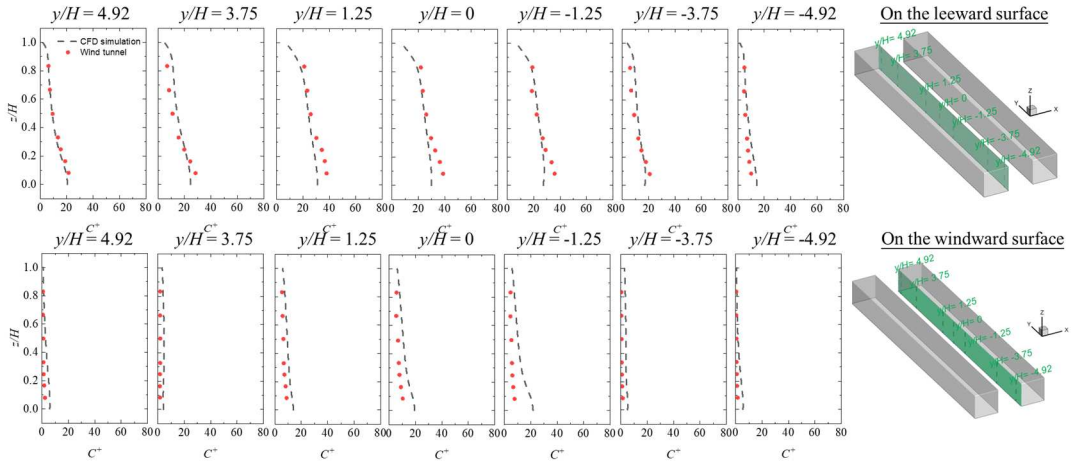
y/H = 4.92
y/H = 3.75
y/H = 1.25
y/H = 0
y/H = -1.25
y/H = -3.75
y/H = -4.92
On the leeward surface
On the windward surface
CFD simulation
Wind tunnel
z/H
C+

(c)

Figure A7 Comparison of WT results and the simulated (a) u/U_{ref} and v/U_{ref} the along three horizontal lines on the vertical corner plane, (b) u/U_{ref} and w/U_{ref} along three horizontal lines on the vertical central plane, and (c) C^+ along 14 vertical lines on the leeward and windward building surfaces

Table A1 Experimental values of pollution source intensity at different times during one day (Ming et al., 2018)

	Time	Morning	Evening	Noon	Other Times
		6:00–8:30	17:30–20:00	11:30–13:00	8:30–11:30 13:00–17:30
Experimental Value	Traffic flow on the left side (vehicle)	62	30	30	16
	Driving speed on the left side (km/h)	11	25	25	40
	CO emission rate (mg/s)	19.86	22.14	22.15	26.15
	Pollution source intensity on the left side (kg/m^3s)	9.93 × 10−7	5.5 × 10−7	5.5 × 10−7	3.3 × 10−7
	Traffic flow on the right side (vehicle)	28	72	30	16
	Driving speed on the right side (km/h)	25	11	25	40
	CO emission rate (mg/s)	22.14	19.86	22.15	26.15
	Pollution source intensity on the right side (kg/m^3s)	5.54 × 10−7	1.15 × 10−6	5.5 × 10−7	3.3 × 10−7

Acknowledgements

This research was supported by the National Natural Science Foundation of China (Grant No. 52278123), the European Commission H2020 Marie S Curie Research and Innovation Staff Exchange (RISE) award (Grant No. 871998). Besides, the authors would like to acknowledge Dr. Christof Bernhard Gromke for help on wind tunnel experiment data for validation.

Reference

Ampountolas, K., Santos, J.A. dos, Carlson, R.C., 2020. Motorway Tidal Flow Lane Control. IEEE Trans. Intell. Transp. Syst. 21, 1687–1696. https://doi.org/10.1109/TITS.2019.2945910

Anjum, S.S., Noor, R.M., Aghamohammadi, N., Ahmedy, I., Kiah, L.M., Hussin, N., Anisi, M.H., Qureshi, M.A., 2019. Modeling Traffic Congestion Based on Air Quality for Greener Environment: An Empirical Study. IEEE Access 7, 57100–57119. https://doi.org/10.1109/ACCESS.2019.2914672

Baik, J.-J., Kang, Y.-S., Kim, J.-J., 2007. Modeling reactive pollutant dispersion in an urban street canyon. Atmos. Environ. 41, 934–949. https://doi.org/https://doi.org/10.1016/j.atmosenv.2006.09.018

Barth, T., Jespersen, D., 1989. The design and application of upwind schemes on unstructured meshes, in: 27th Aerospace Sciences Meeting. p. 366.

Buccolieri, R., Gromke, C., Di Sabatino, S., Ruck, B., 2009. Aerodynamic effects of trees on pollutant concentration in street canyons. Sci. Total Environ. 407, 5247–5256. https://doi.org/https://doi.org/10.1016/j.scitotenv.2009.06.016

Cai, C., Ming, T., Fang, W., de Richter, R., Peng, C., 2020a. The effect of turbulence induced by different kinds of moving vehicles in street canyons. Sustain. Cities Soc. 54, 102015. https://doi.org/https://doi.org/10.1016/j.scs.2020.102015

Cai, C., Ming, T., Fang, W., de Richter, R., Peng, C., 2020b. The effect of turbulence induced by different kinds of moving vehicles in street canyons. Sustain. Cities Soc. 54, 102015. https://doi.org/10.1016/J.SCS.2020.102015

Chen, D., Yan, X., Liu, F., Liu, X., Wang, L., Zhang, J., 2019. Evaluating and diagnosing road intersection operation performance using floating car data. Sensors 19, 2256.

Chew, L.W., Aliabadi, A.A., Norford, L.K., 2018. Flows across high aspect ratio street canyons: Reynolds number independence revisited. Environ. Fluid Mech. 18, 1275–1291.

Fluent, A., 2013. ANSYS fluent theory guide 15.0. Inc, Canonsburg, PA.

Franke, J., Hellsten, A., Schlunzen, K.H., Carissimo, B., 2011. The COST 732 Best Practice Guideline for CFD simulation of flows in the urban environment: a summary. Int. J. Environ. Pollut. 44, 419–427. https://doi.org/10.1504/IJEP.2011.038443

Grimmond, S., 2007. Urbanization and global environmental change: local effects of urban warming. Geogr. J. 173, 83–88.

Gromke, C., 2013. CODASC: a database for the validation of street canyon dispersion models, in: The 15th International Conference on Harmonisation within Atmospheric Dispersion Modelling for Regulatory Purposes (HARMO).

Gromke, C., Ruck, B., 2007. Influence of trees on the dispersion of pollutants in an urban street canyon—experimental investigation of the flow and concentration field. Atmos. Environ. 41, 3287–3302.

Hang, J., Li, Y., Buccolieri, R., Sandberg, M., Di Sabatino, S., 2012. On the contribution of mean flow and turbulence to city breathability: the case of long streets with tall buildings. Sci. Total Environ. 416, 362–373.

Hayati, A.N., Stoll, R., Pardyjak, E.R., Harman, T., Kim, J.J., 2019. Comparative metrics for computational approaches in non-uniform street-canyon flows. Build. Environ. 158, 16–27. https://doi.org/https://doi.org/10.1016/j.buildenv.2019.04.028

Hu, X., Lin, C., Hao, X., Lu, R., Liu, T., 2021. Influence of tidal lane on traffic breakdown and spatiotemporal congested patterns at moving bottleneck in the framework of Kerner's three-phase traffic theory. Phys. A Stat. Mech. its Appl. 584, 126335. https://doi.org/https://doi.org/10.1016/j.physa.2021.126335

Issakhov, A., Omarova, P., 2021. Modeling and analysis of the effects of barrier height on automobiles emission dispersion. J. Clean. Prod. 296, 126450. https://doi.org/https://doi.org/10.1016/j.jclepro.2021.126450

Kastner-Klein, P., Berkowicz, R., Plate, E.J., 2000. Modelling of vehicle-induced turbulence in air pollution studies for streets. Int. J. Environ. Pollut. 14, 496–507.

Kondo, H., Tomizuka, T., 2009. A numerical experiment of roadside diffusion under traffic-produced flow and turbulence. Atmos. Environ. 43, 4137–4147.

Li, Q., Chen, C., Deng, Y., Li, J., Xie, G., Li, Y., Hu, Q., 2015. Influence of traffic force on pollutant dispersion of CO, NO and particle matter (PM2.5) measured in an urban tunnel in Changsha, China. Tunn. Undergr. Sp. Technol. 49, 400–407. https://doi.org/https://doi.org/10.1016/j.tust.2015.04.019

Li, X.-X., Liu, C.-H., Leung, D.Y.C., 2009. Numerical investigation of pollutant transport characteristics inside deep urban street canyons. Atmos. Environ. 43, 2410–2418.

Li, Z., Ming, T., Liu, S., Peng, C., de Richter, R., Li, W., Zhang, H., Wen, C.-Y., 2021a. Review on pollutant dispersion in urban areas-part A: Effects of mechanical factors and urban morphology. Build. Environ. 190, 107534. https://doi.org/https://doi.org/10.1016/j.buildenv.2020.107534

Li, Z., Shi, T., Wu, Y., Zhang, H., Juan, Y.-H., Ming, T., Zhou, N., 2020. Effect of traffic tidal flow on pollutant dispersion in various street canyons and corresponding mitigation strategies. Energy Built Environ. 1, 242–253. https://doi.org/https://doi.org/10.1016/j.enbenv.2020.02.002

Li, Z., Xu, J., Ming, T., Peng, C., Huang, J., Gong, T., 2017. Numerical simulation on the effect of vehicle movement on pollutant dispersion in urban street. Procedia Eng. 205, 2303–2310.

Li, Z., Zhang, H., Wen, C.-Y., Yang, A.-S., Juan, Y.-H., 2021b. The effects of lateral entrainment on pollutant dispersion inside a street canyon and the corresponding optimal urban design strategies. Build. Environ. 195, 107740. https://doi.org/https://doi.org/10.1016/j.buildenv.2021.107740

Mazzeo, N.A., Venegas, L.E., 2005. 5.22 EVALUATION OF TURBULENCE FROM TRAFFIC USING EXPERIMENTAL DATA OBTAINED IN A STREET CANYON.

Ming, T., Davies, P., Liu, W., Caillol, S., 2017. Removal of non-CO2 greenhouse gases by large-scale atmospheric solar photocatalysis. Prog. Energy Combust. Sci. 60, 68–96.

Ming, T., Fang, W., Peng, C., Cai, C., De Richter, R., Ahmadi, M.H., Wen, Y., 2018. Impacts of traffic tidal flow on pollutant dispersion in a non-uniform urban street canyon. Atmosphere (Basel). 9, 82.

Mochida, A., Lun, I.Y.F., 2008. Prediction of wind environment and thermal comfort at pedestrian level in urban area. J. Wind Eng. Ind. Aerodyn. 96, 1498–1527. https://doi.org/https://doi.org/10.1016/j.jweia.2008.02.033

Mochida, A., Lun, Y.F., 2006. Prediction of wind environment and thermal comfort at pedestrian level in urban area. J. Wind Eng. Ind. Aerodyn. 96.

Ng, W.-Y., Chau, C.-K., 2014. A modeling investigation of the impact of street and building configurations on personal air pollutant exposure in isolated deep urban canyons. Sci. Total Environ. 468–469, 429–448. https://doi.org/https://doi.org/10.1016/j.scitotenv.2013.08.077

Peng, C., Ming, T., gui, J., Tao, Y., Peng, Z., 2015. Numerical analysis on the thermal environment of an old city district during urban renewal. Energy Build. 89, 18–31. https://doi.org/https://doi.org/10.1016/j.enbuild.2014.12.023

Pospisil, J., Jicha, M., 2010. Particulate matter dispersion modelling along urban traffic paths. Int. J. Environ. Pollut. 40, 26–35.

Rakowska, A., Wong, K.C., Townsend, T., Chan, K.L., Westerdahl, D., Ng, S., Močnik, G., Drinovec, L., Ning, Z., 2014. Impact of traffic volume and composition on the air quality and pedestrian exposure in urban street canyon. Atmos. Environ. 98, 260–270. https://doi.org/https://doi.org/10.1016/j.atmosenv.2014.08.073

Rastetter, A., 1997. Experimentelle Untersuchung in einem atmosphärischen Grenzschichtwindkanal über den Einfluß von Kfz-erzeugter Turbulenz auf die Schadstoffausbreitung in Straßenschluchten.

Roache, P.J., 1997. Quantification of uncertainty in computational fluid dynamics. Annu. Rev. Fluid Mech. 29, 123–160.

Rückerl, R., Schneider, A., Breitner, S., Cyrys, J., Peters, A., 2011. Health effects of particulate air pollution: a review of epidemiological evidence. Inhal. Toxicol. 23, 555–592.

Sahlodin, A.M., Sotudeh-Gharebagh, R., Zhu, Y., 2007. Modeling of dispersion near roadways based on the vehicle-induced turbulence concept. Atmos. Environ. 41, 92–102.

Salim, S.M., Buccolieri, R., Chan, A., Di Sabatino, S., 2011. Numerical simulation of atmospheric pollutant dispersion in an urban street canyon: Comparison between RANS and LES. J. Wind Eng. Ind. Aerodyn. 99, 103–113. https://doi.org/https://doi.org/10.1016/j.jweia.2010.12.002

Shi, T., Ming, T., Wu, Y., Peng, C., Fang, Y., de_Richter, R., 2020. The effect of exhaust emissions from a group of moving vehicles on pollutant dispersion in the street canyons. Build. Environ. 181, 107120. https://doi.org/https://doi.org/10.1016/j.buildenv.2020.107120

Shi, Y., Xie, X., Fung, J.C.-H., Ng, E., 2018. Identifying critical building morphological design factors of street-level air pollution dispersion in high-density built environment using mobile monitoring. Build. Environ. 128, 248–259. https://doi.org/https://doi.org/10.1016/j.buildenv.2017.11.043

Snyder, W.H., 1972. Similarity criteria for the application of fluid models to the study of air pollution meteorology. Boundary-Layer Meteorol. 3, 113–134. https://doi.org/10.1007/BF00769111

Tan, Z., Dong, J., Xiao, Y., Tu, J., 2015. A numerical study of diurnally varying surface temperature on flow patterns and pollutant dispersion in street canyons. Atmos. Environ. 104, 217–227. https://doi.org/https://doi.org/10.1016/j.atmosenv.2015.01.027

Thaker, P., Gokhale, S., 2016. The impact of traffic-flow patterns on air quality in urban street canyons. Environ. Pollut. 208, 161–169.

Tominaga, Y., Mochida, A., Yoshie, R., Kataoka, H., Nozu, T., Yoshikawa, M., Shirasawa, T., 2008. AIJ guidelines for practical applications of CFD to pedestrian wind environment around buildings. J. Wind Eng. Ind. Aerodyn. 96, 1749–1761. https://doi.org/https://doi.org/10.1016/j.jweia.2008.02.058

Tominaga, Y., Stathopoulos, T., 2007. Turbulent Schmidt numbers for CFD analysis with various types of flowfield. Atmos. Environ. 41, 8091–8099. https://doi.org/https://doi.org/10.1016/j.atmosenv.2007.06.054

Wai, W.T., San, W.T.W., Shun, M., Hon, A.L.K., Ng, M.S.K.W., Yeung, M.D., Ming, W.C., 2012. A study of the air pollution index reporting system. Stat. Modelling 13, 15.

Wang, H., Peng, C., Li, W., Ding, C., Ming, T., Zhou, N., 2021. Porous media: A faster numerical simulation method applicable to real urban communities. Urban Clim. 38, 100865. https://doi.org/https://doi.org/10.1016/j.uclim.2021.100865

Wang, Q., Fang, W., de Richter, R., Peng, C., Ming, T., 2019. Effect of moving vehicles on pollutant dispersion in street canyon by using dynamic mesh updating method. J. Wind Eng. Ind. Aerodyn. 187, 15–25.

Wang, Y.J., Zhang, K.M., 2009. Modeling Near-Road Air Quality Using a Computational Fluid Dynamics Model, CFD-VIT-RIT. Environ. Sci. Technol. 43, 7778–7783. https://doi.org/10.1021/es9014844

Weerasuriya, A.U., Zhang, X., Tse, K.T., Liu, C.-H., Kwok, K.C.S., 2022. RANS simulation of near-field dispersion of reactive air pollutants. Build. Environ. 207, 108553. https://doi.org/https://doi.org/10.1016/j.buildenv.2021.108553

Who, 2014. Ambient (outdoor) air quality and health. WHO Media Cent.

Xia, Y., Guan, D., Jiang, X., Peng, L., Schroeder, H., Zhang, Q., 2016. Assessment of socioeconomic costs to China's air pollution. Atmos. Environ. 139, 147–156. https://doi.org/https://doi.org/10.1016/j.atmosenv.2016.05.036

Yang, H., Lam, C.K.C., Lin, Y., Chen, L., Mattsson, M., Sandberg, M., Hayati, A., Claesson, L., Hang, J., 2021. Numerical investigations of Re-independence and influence of wall heating on flow characteristics and ventilation in full-scale 2D street canyons. Build. Environ. 189, 107510. https://doi.org/https://doi.org/10.1016/j.buildenv.2020.107510

Yao, R., Zhang, X., Wu, N., Song, X., 2018. Modeling and control of variable approach lanes on an arterial road: A case study of Dalian. Can. J. Civ. Eng. 45, 986–1003.

Zhao, Y., Jiang, C., Song, X., 2021. Numerical evaluation of turbulence induced by wind and traffic, and its impact on pollutant dispersion in street canyons. Sustain. Cities Soc. 74, 103142. https://doi.org/https://doi.org/10.1016/j.scs.2021.103142

Zheng, X., Montazeri, H., Blocken, B., 2021. Large-eddy simulation of pollutant dispersion in generic urban street canyons: Guidelines for domain size. J. Wind Eng. Ind. Aerodyn. 211, 104527. https://doi.org/https://doi.org/10.1016/j.jweia.2021.104527

Zheng, X., Yang, J., 2022. Impact of moving traffic on pollutant transport in street canyons under perpendicular winds: A CFD analysis using large-eddy simulations. Sustain. Cities Soc. 82, 103911. https://doi.org/https://doi.org/10.1016/j.scs.2022.103911

Zheng, X., Yang, J., 2021. CFD simulations of wind flow and pollutant dispersion in a street canyon with traffic flow: Comparison between RANS and LES. Sustain. Cities Soc. 75, 103307. https://doi.org/https://doi.org/10.1016/j.scs.2021.103307

Zhou, S., Lin, R., 2019. Spatial-temporal heterogeneity of air pollution: The relationship between built environment and on-road PM2.5 at micro scale. Transp. Res. Part D Transp. Environ. 76, 305–322. https://doi.org/https://doi.org/10.1016/j.trd.2019.09.004